Circulation

ORIGINAL RESEARCH ARTICLE

An Aberrant Resurgence of Endogenous Retroviruses Prompts Myocarditis and Heart Failure

Junhao Xiong, BS*; Shasha Zhang, PhD*; Zilong Geng, BS*; Juntao Lin, BS*; Kang Cheng, BS; Huan Hu, BS; Yuze Wang, BS; Xing Liu, BS; Yuanzhe Sheng, BS; Ping Yang, PhD; Yige Li, BS; Shuo Wu, BS; Xiao Cheng, PhD; Yelan Li, BS; Aijun Sun, PhD; Alex F. Chen, PhD; Daowen Wang, PhD; Chen Chen, PhD; Yan Zhang, PhD; Gengze Wu, PhD; Chunyu Zeng, PhD; Xiaoling Guo, PhD; Xumin Hou, PhD; Ruogu Li, PhD; Yuliang Feng, PhD; Dan Zhu, PhD; Kun Sun, PhD; Bing Zhang, PhD

BACKGROUND: Endogenous retroviruses (ERVs) occupy >8% of the human genome. Aberrant resurgence of ERVs has been implicated recently in several critical pathologies. However, the possible incidence and role of ERV resurgence in heart failure (HF), a leading cause of global morbidity and mortality, remain unexplored.

METHODS: We established a total RNA sequencing analyzing pipeline to assess the ERV occurrence in human and murine HF models. We generated 2 myocardium-specific mouse lines by crossing *Myh6*-MerCreMer with TRIM28$^{f/f}$ and SETDB1$^{f/f}$ mice to identify the molecular regulators of ERV resurgence and the downstream pathways in the heart. We evaluated ERV expression by total RNA sequencing, reverse transcription-quantitative polymerase chain reaction and RNA fluorescence in situ hybridization. We restrained ERV activation by overexpressing TRIM28 (tripartite motif–containing 28) using adeno-associated virus serotype 9. The therapeutic potential of the ERV-mediated inflammatory pathway was tested in a myocardial ischemia/reperfusion model.

RESULTS: ERVs, particularly class I ERVs, were prominently activated in multiple cross-species models of HF. Depletion of TRIM28, an epigenetic repressor, attenuated the epigenetic surveillance of trimethylation at lysine 9 of histone H3 and N^6-methyladenosine, leading to the activation of ERVs in the failing heart. This ERV activation stimulated the antiviral innate immune pathways of TLR7/9 (Toll-like receptor 7/9) and NF-κB and lead to myocarditis and acute HF. Furthermore, restraining ERV activation and ERV-mediated innate immune responses by either adeno-associated virus serotype 9–mediated TRIM28 expression or a small-molecule TLR7/9 inhibitor improved heart function and alleviated HF in an ischemia/reperfusion model.

CONCLUSIONS: ERV resurgence is a specific molecular trait of HF, driven by TRIM28 depletion in cardiomyocytes. ERV resurgence activates the innate immune TLR7/9–NF-κB pathway and induces myocarditis and HF. Inception of ERVs and the ERV-mediated immune pathway confers cardiac protection. These results identify TRIM28–ERV–TLR7/9–NF-κB as a target for therapeutic management of myocarditis and HF.

Key Words: endogenous retrovirus ■ heart failure ■ myocarditis ■ NF-κB ■ TRIM28

Correspondence to: Bing Zhang, PhD, Key Laboratory of Systems Biomedicine, Shanghai Center for Systems Biomedicine, Department of Cardiovascular Surgery, Shanghai Chest Hospital, Engineering Research Center of Techniques and Instruments for Diagnosis and Treatment of Congenital Heart Disease, Institute of Developmental and Regenerative Medicine, Xinhua Hospital, School of Medicine, Shanghai Jiao Tong University, 1555 Kongjiang Rd, Yangpu District, Shanghai, China, 200082, Email bingzhang@sjtu.edu.cn, or Kun Sun, PhD, Key Laboratory of Systems Biomedicine, Shanghai Center for Systems Biomedicine, Department of Cardiovascular Surgery, Shanghai Chest Hospital, Engineering Research Center of Techniques and Instruments for Diagnosis and Treatment of Congenital Heart Disease, Institute of Developmental and Regenerative Medicine, Xinhua Hospital, School of Medicine, Shanghai Jiao Tong University, 1555 Kongjiang Rd, Yangpu District, Shanghai, China, 200082, Email sunkun@xinhuamed.com.cn, or Dan Zhu, PhD, Key Laboratory of Systems Biomedicine, Shanghai Center for Systems Biomedicine, Department of Cardiovascular Surgery, Shanghai Chest Hospital, Engineering Research Center of Techniques and Instruments for Diagnosis and Treatment of Congenital Heart Disease, Institute of Developmental and Regenerative Medicine, Xinhua Hospital, School of Medicine, Shanghai Jiao Tong University, 1555 Kongjiang Rd, Yangpu District, Shanghai, China, 200082, Email zhudanmd@163.com
*J. Xiong, S. Zhang, Z. Geng, and J. Lin contributed equally.
Supplemental Material is available with this article at https://www.ahajournals.org/doi/suppl/10.1161/CIRCULATIONAHA.125.074845.
For Sources of Funding and Disclosures, see page XXX.

Circulation is available at www.ahajournals.org/journal/circ

Clinical Perspective

What Is New?

- Endogenous retroviruses (ERVs), particularly class I ERVs, are activated in multiple cross-species models of heart failure (HF).
- ERV resurgence in cardiomyocytes stimulates the innate immune pathways of TLR7/9 (Toll-like receptor 7/9) and NF-κB and results in severe myocarditis and acute HF.
- Suppressing the innate immune responses by adeno-associated virus serotype 9-TRIM28 (tripartite motif–containing protein 28) or using the TLR7/9 inhibitor NSC4375 protects against myocarditis and HF after ischemia/reperfusion.

What Are the Clinical Implications?

- ERV resurgence driven by TRIM28 depletion is associated with the occurrence of HF.
- ERV hyperactivation causes myocarditis and acute HF in a mouse model that resembles fulminant myocarditis in the clinic.
- Intervening in the aberrant activation of the TRIM28–ERV–TLR7/9–NF-κB pathway may be a novel therapeutic approach for myocarditis and HF management.

Nonstandard Abbreviations and Acronyms

AAV9	adeno-associated virus serotype 9
AHF	acute heart failure
DCM	dilated cardiomyopathy
ERV	endogenous retrovirus
ERV1	endogenous retrovirus class 1
H3K9me3	trimethylation at lysine 9 of histone H3
HERV	human endogenous retrovirus
HF	heart failure
I/R	ischemia/reperfusion
LINE	long interspersed element
LTR	long terminal repeat
m6A	N^6-methyladenosine
RNA-seq	RNA sequencing
RTE	retrotransposon element
RTi	reverse transcriptase inhibitor
SINE	short interspersed element
upERV	upregulated endogenous retrovirus

Heart failure (HF) is a prevalent syndrome characterized by the inability of the heart to pump sufficient blood to meet the needs of the body. HF affects >64 million people worldwide, making it a leading cause of global morbidity and mortality.[1] Because of a lack of effective treatment, the 5-year mortality of HF exceeds 50%[1] and is worse than for most types of cancers. Acute HF (AHF) is the most deleterious subtype of HF, characterized by the sudden onset of HF or rapid deterioration of pre-existing HF, with a 1-year mortality rate of ≈30%.[2] Myocarditis, especially fulminant myocarditis, is a common underlying cause of AHF and often caused by exogenous virus infections, such as coxsackie virus B, adenoviruses, parvovirus B19, herpes viruses, HIV, and SARS-CoV-2 (eg, COVID-19).[3,4] However, the potential role of endogenous viruses, endogenized and integrated proviruses composed of transposons in the host genome, remains largely unexplored.

The mammalian genome contains a vast array of transposons classified into DNA transposons and retrotransposons based on their intermediates.[5] Retrotransposons without long terminal repeats (LTRs), including autonomous long interspersed elements (LINEs) and nonautonomous short interspersed elements (SINEs), require LINE-derived proteins for mobilization. Retrotransposons with LTRs are predominantly endogenous retroviruses (ERVs) comprising approximately 8% of the human genome and 10% of the mouse genome.[6,7] Among them, less than 10% are full-length ERVs, containing 4 basic viral packaging genes (*gag*, *pol*, *env*, and *pro*), which is similar to exogenous retroviruses,[5,7] and are capable of forming active virus particles. In contrast, >90% of ERVs are defective because of accumulated mutations and stop codons embedded in the host genome. Nevertheless, even defective ERVs may still transcribe RNA because of the promoter function buried in their LTRs, potentially leading to immune responses and disease. Therefore, ERVs represent the most functional class of retrotransposons. Human ERVs (HERVs) and rodent ERVs are classified into 3 classes (class I [ERV1], class II [ERVK], and class III [ERVL]) based on their clustering with lentiviruses, retroviruses, and spumaviruses, respectively. Emerging evidence indicates that the changes in HERV activity at the DNA or RNA levels influence embryonic development and somatic tissue homeostasis. Concurrently, aberrant HERV activation has been implicated in human pathological conditions, including neurodegenerative disorders, autoimmune inflammation, and tumorigenesis.[8–10] However, a definitive correlation between specific HERV subtypes and human diseases has yet to be established, particularly for cardiovascular disease and HF.

To maintain genomic stability, ERVs are required to be meticulously silenced by multiple genetic and epigenetic mechanisms.[7,9] TRIM28 (tripartite motif–containing protein 28) is a transcriptional repressor with a pivotal role in maintaining heterochromatin. The N-terminal RBCC domain of TRIM28 interacts with KRAB-ZNPs to facilitate TRIM28 recruitment to the heterochromatin. The C-terminal PHD domain and bromodomain of TRIM28 accommodates SETDB1, a histone H3 methyltransferase, which catalyzes the H3K9me2 or trimethylation at

lysine 9 of histone H3 (H3K9me3) methylation of histone H3.[11,12] TRIM28 is a critical regulator of embryonic stem cell pluripotency and organismal development.[12,13] Mice deficient in TRIM28 die early before gastrulation.[14] TRIM28 inhibits the expression of several types of retroviruses, including HIV, and their integration inside the host cells.[15] TRIM28 has also been shown to maintain the surveillance of endogenous viruses in embryonic stem cells, neural progenitor cells, and aged tissues.[16–18] Our previous study reported that TRIM28 regulates endothelium-to-mesenchymal transition and heart valve development.[19] However, its function in cardiomyocytes and the adult heart and whether it can silence remain unknown.

In this study, we uncovered that ERVs, particularly class I, were specifically activated in human, nonhuman primate, and rodent HF models. We further identified TRIM28 as the key player responsible for ERV activation by manipulating 2 distinctive types of epigenetic modifications: H3K9me3 and RNA N^6-methyladenosine (m^6A). Increased ERVs in cardiomyocytes trigger the pattern recognition receptors TLR7/9 (Toll-like receptor 7/9) and the NF-κB pathway rather than the classical IFN (interferon) pathway, leading to myocarditis and AHF. Suppressing ERV activation in the myocardium using associated virus serotype 9 (AAV9)-TRIM28 or inhibiting the TLR7/9 pathway with the small-molecule inhibitor NSC4375 effectively mitigated inflammation and protected against ischemia/reperfusion (I/R)–induced HF. Collectively, our findings showed a critical role of ERV resurgence and identified TRIM28–ERV–TLR7/9–NF-κB as a new molecular axis driving the pathogenesis of myocarditis and HF.

METHODS

Human Samples

Human control (CTR) and dilated cardiomyopathy (DCM) heart samples were procured from Tongji Hospital (Wuhan, China) as described previously,[20] in accordance with the ethics standards of the Declaration of Helsinki. The study was conducted with the express approval of the ethics review board of Tongji Hospital and Tongji Medical College. Before sample collection, informed consent was obtained from the patients or their legally authorized representatives.

Mice

The TRIM28$^{flox/flox}$ mice were purchased from Biocytogen Pharmaceuticals Co Ltd (Beijing, China). The SETDB1$^{flox/flox}$ mice were provided by the Jiekai Chen group.[21] The TRIM28^{iCKO} and SETDB1^{iCKO} mice were generated by crossing TRIM28$^{flox/flox}$ or SETDB1$^{flox/flox}$ mice with Myh6-MerCreMer mice, and the genomic deletion of TRIM28 or SETDB1 was introduced via intraperitoneal administration of 25 mg/kg of tamoxifen dissolved in corn oil for 5 consecutive days. The animals were maintained under standard photoperiod conditions (12-hour light/dark cycle). All experimental procedures were conducted in accordance with the guidelines of the institutional animal care and use committee of Shanghai Jiao Tong University. Animal studies adhered to the Animal Research: Reporting of In Vivo Experiments guidelines. The sample size was estimated by previous related studies and set to be a minimal requirement matching statistical power (0.8) and alpha (0.05). Animals were randomly assigned to receive AAV9 or drug treatments. The experimental operators were blinded to the treatment plans.

Statistical Analysis

Statistical analysis was performed with GraphPad Prism 9.0 or R Studio. Data normality was estimated with the Shapiro-Wilk normality test preceding the significance analysis, and $P \geq 0.05$ was considered a normal distribution. Two-group data in normal distribution were analyzed with 2-tailed unpaired parametric *t* test and otherwise with the Mann-Whitney *U* test. For a multiple-group comparison, 1-way ANOVA followed by Tukey post hoc test was used if the data were normally distributed; otherwise, the nonparametric Kruskal-Wallis test with Dunn multiple comparisons test was employed. Two-way ANOVA with post hoc Sidak multiple comparison test was used to analyze data with 2 independent variables. Mixed-effects ANOVA test was used to analyze data with serial measurements on the same mice. A log-rank test was used for the survival analysis. The data are presented as mean±SD, and $P<0.05$ was set as statistical significance.

Data Availability

All next-generation sequencing data are accessible in the GEO repository (GSE274895). The data, protocols, and study materials that support the findings of this study are available from the corresponding author upon request.

RESULTS

ERV Resurgence in Human and Animal HF Models

To explore the possible role of retrotransposon elements (RTEs) in HF, we analyzed the published data sets of RNA sequencing (RNA-seq) from NCBI GEO with the following inclusion criteria: (1) human ventricle samples, (2) clear HF diagnosis (NYHA III–IV), (3) sample size >20, and (4) total RNA-seq data. Three data sets met these criteria (GSE135055, DCM; GSE126569, DCM; and GSE48166, ischemic cardiomyopathy),[22] which were retrieved as clustered and high-quality data from a total of 42 HF patients and 36 healthy donors, by principal component analysis and followed by a custom RTE calling pipeline (Figure 1A; Figure S1A through S1C). Their clinical characteristics are summarized in Table S1. Among all RTEs, only LTR-containing ERVs showed significant upregulation in HF patients (GSE135055, $P=0.0002$; GSE126569, $P=0.009$; GSE48166, $P=0.0008$; Figure 1B; Figure S1D through S1H) and accounted for 76% (74 of 97) of all differentially expressed RTEs (Table S2). Among 4 ERV subfamilies (HERV1, HERVK, HERVL,

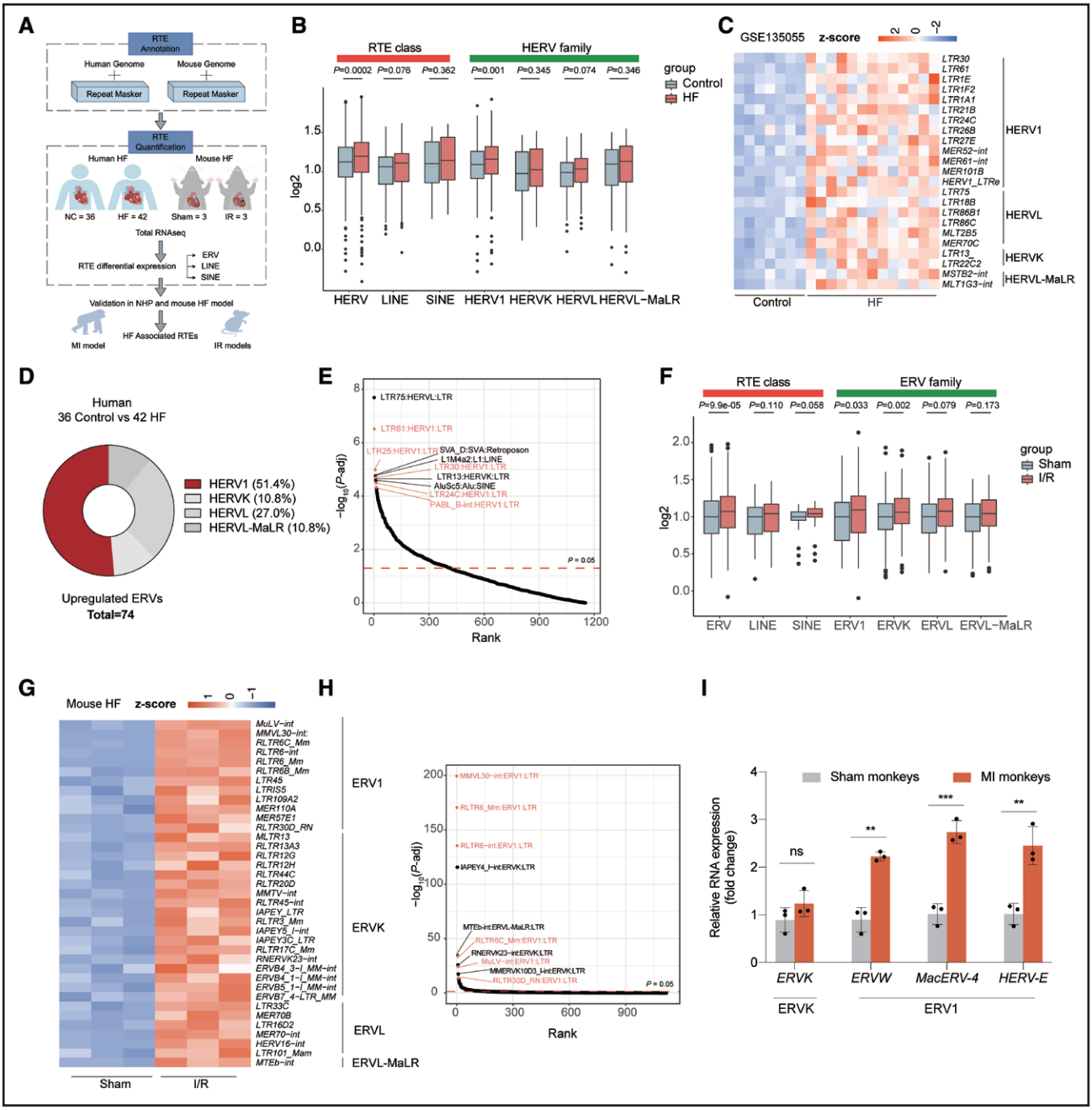

Figure 1. A retroviral provirus revives in heart failure.

A, The scheme for the discovery of heart failure (HF)–associated retrotransposon elements (RTEs) in cross-species HF models. RTE sequences were annotated using Repeat Masker across multiple species. Differentially expressed RTEs were identified from total RNA sequencing using DESeq2, some of which were further validated by RT-qPCR. **B**, Boxplots showing human endogenous retroviruses (HERVs), especially HERV1, increased in GSE135055 human HF hearts. The center line indicates the median. The box indicates 25th and 75th percentiles; n=7 controls and 13 HF patients. Mann-Whitney test was used to calculate the significance. **C**, Heatmap presenting the significantly elevated HERV genes in human HF hearts (adjusted *P* [*P*-adj]<0.05, fold change>0.5). Data were from the GEO database (GSE135055). There were 7 control patients and 13 HF patients. **D**, Ring plots showing the percentages of 74 upregulated endogenous retroviruses (ERVs) in each family identified from human GEO data sets (GSE135055, GSE126569, and GSE48166). **E**, *P*-adj value ranking identified HERV1 as the most significantly altered HERVs in human HF (threshold: *P*-adj=0.05, denoted by a dotted line). HERV1 genes LTR61, LTR25, LTR30, LTR24C, and PABL_B-int were among the top 10 differentially expressed HF RTEs. *P*-adj was calculated with the DESeq2 package, and Benjamini-Hochberg adjustment was used to control the false positives in multiple testing. **F**, Boxplots indicating the upregulation of mouse ERVs, especially ERV1, in ischemia/reperfusion injury hearts. The center line indicates the median. The box indicates 25th and 75th percentiles; n=3 mice per group. Mann-Whitney test. **G**, Heatmap showing the resurgence of mouse ERVs in ischemia/reperfusion injury hearts in the analysis of total RNA sequencing (*P*-adj<0.05, fold change>1.5). n=3 mice per group. **H**, *P*-adj value ranking implicating ERV1 as the most significantly altered ERVs in ischemia/reperfusion mouse hearts. The dotted line indicates *P*-adj=0.05. MMVL30-int, RLTR6_Mm, RLTR6-int, RLTR6C_Mm, MuLV-int, and RLTR30D_RN, in red, belong to the mouse ERV1 family with top 10 ranking in differentially expressed retrotransposons. (*Continued*)

Figure 1 Continued. **I**, RT-qPCR showing the resurgence of ERVs in monkey hearts 4 weeks after myocardial infarction. ERVW, MacERV-4 and HERV-E belong to ERVI RTE genes, whereas ERVK was ERVII. Data are mean±SD; n=3 hearts per group. Two-tailed Student *t* test; ***P*<0.01, ****P*<0.001o significance. I/R indicates ischemia/reperfusion; MI, myocardial infarction; NC, negative control; NHP, nonhuman primate; ns, no significance; and RT-qPCR, reverse transcription-quantitative polymerase chain reaction.

and HMaLR), HERV1 was the only subfamily consistently and significantly upregulated across all 3 data sets (GSE135055, *P*=0.0007; GSE126569, *P*=0.033; GSE48166, *P*=0.0027; Figure 1B; Figures S1D and S1E). Consistent with this, 74 ERV genes were upregulated in failing hearts, with the majority (n=38, 51.4%) belonging to the HERV1 subfamily (Figure 1C and 1D; Figure S1I and S1J). Ranking the differential expression of ERVs further confirmed the dominance of HERV1 RTEs among resurrected ERVs (Figure 1E; Figure S1K and S1L; Table S3). Although most of ERV1 is unable to form infectious viral particles, some members, such as HERV-H[23] and HERV-W[24] in ERV1, have been reported previously to be associated with neurodegeneration and inflammatory disorders, implying potent functionality of ERV1. In contrast, although some young subfamilies, such as ERVK, can generate living virus and have been linked to the pathologies of neural diseases, systemic lupus erythematosus, and cancer,[25] their viral load in the human HF heart samples were very low (Figure S1M and S1N) and similar to the CTR (*P*=0.3628). This finding aligned with the RNA-seq data, suggesting that ERVK does not play a major role in HF pathogenesis.

To further validate ERV resurgence in HF, we analyzed ERV expression in a mouse I/R model (Figure S1O). Consistent with human data, ERVs were significantly upregulated in I/R hearts compared with other RTEs (Figure 1F). Although both ERV1 and ERVK were upregulated (Figure 1F), the increase in ERV1 was more pronounced (Figure 1G and 1H; Table S3). The most significantly upregulated RTE genes were MMVL30-int (adjusted P [*P*-adj]=2.52e−200) and RLTR6_Mm (*P*-adj=2.68e−171), both belonging to the ERV1 family (Figure 1H; Table S3), and their biological functions remain unexplored. The resurgence of ERV1 rather than ERVK was also discovered in nonhuman primate myocardial infarction HF models using reverse transcription-quantitative polymerase chain reaction (Figure 1I). Together, these results identified the resurgence of ERVs, particularly ERV1, as a potential molecular feature of HF across 3 species.

TRIM28 Deprivation Led to the Resurgence of ERV and AHF

Repressive epigenetic modification is the major mechanism silencing the transcription of genomic ERVs.[7,8,26] TRIM28 functions as a master regulator orchestrating epigenetic repression and plays an important role in the surveillance of endogenous and exogenous viruses.[11,12] We found that TRIM28 was notably downregulated in human HF specimens, indicating that it might be involved in ERV reactivation in HF (Figure 2A and 2B; Figure S2A; Table S1). To investigate further, we generated an inducible cardiomyocyte-specific TRIM28 deletion mouse Myh6-MerCreMer: TRIM28$^{f/f}$ (TRIM28^{iCKO}) mice, by crossing TRIM28 flox mice with Myh6-MerCreMer mice (Figure S2B through S2D). Total RNA-seq showed that, compared with wild-type hearts, 12 ERV genes were significantly upregulated in TRIM28^{iCKO} hearts, many more than LINE and SINE (3 and 0 genes, respectively; Figure 2C). Several ERVK genes were also upregulated, whereas IAPEZ[27] and MMERVK10C,[28] with known functions in immunity, were unaltered (Figure 2C; Figure S2E). Notably, ERV1 was the most dominantly upregulated ERVs (upERVs), comprising half of the elevated ERVs and ranking at the top (Figure 2C and S2D; Table S3).

Akin to the I/R model, the most prominently elevated ERV1 RTEs in TRIM28^{iCKO} hearts were MMVL30-int (*P*-adj=2.32e−24) and RLTR6_Mm (*P*-adj=1.15e−18; Figure 2D; Figure S2F and S2G). Of MMVL3-int, 48.2% (108 of 224) showed an increase >2-fold, and 25.7% (29 of 113) of RLTR6_Mm transcripts showed an increase >2-fold (Figure S2H and S2I; Table S4). MMVL30-int is a nonautonomous ERV flanked by RLTR6_Mm as its LTR elements[29] (Figure 2E) and has been associated with stress responses such as cerebral ischemia.[30] RNA fluorescence in situ hybridization confirmed that MMVL30 RTE RNA indeed increased in TRIM28^{iCKO} cardiomyocytes. MMVL30 appeared as speckles inside the cytosol, suggesting that its primary functional locations in cardiomyocytes might be either endosomes (subcellular organelles for TLR7/9 and the innate immune response)[10] or P-bodies (subcellular organelles for RNA decay;[31] Figure 2F).

Surprisingly, TRIM28^{iCKO} mice started to die only 4 days after tamoxifen induction, and 46% died within 2 weeks (*P*=0.0037; Figure 2G). Echocardiography assessments revealed that systolic function started to decline on day 3 post tamoxifen induction (ejection fraction: 54.88±5.93 versus 33.79±4.59, CTR versus TRIM28^{iCKO}, *P*<0.001), reaching its lowest point on day 7 (ejection fraction: 52.37±3.47 versus 19.81±5.60, CTR versus TRIM28^{iCKO}, *P*<0.001; Figure 2H; Figure S3A and S3B). This change was accompanied by an increase in cardiac chamber size and thinning of the posterior cardiac wall, suggesting DCM-type HF in TRIM28^{iCKO} mice (Figure 2I and 2J; Figure S3A and S3B; Table S5).

Upon dissection of the hearts 7 days post tamoxifen induction, TRIM28^{iCKO} hearts were much larger than

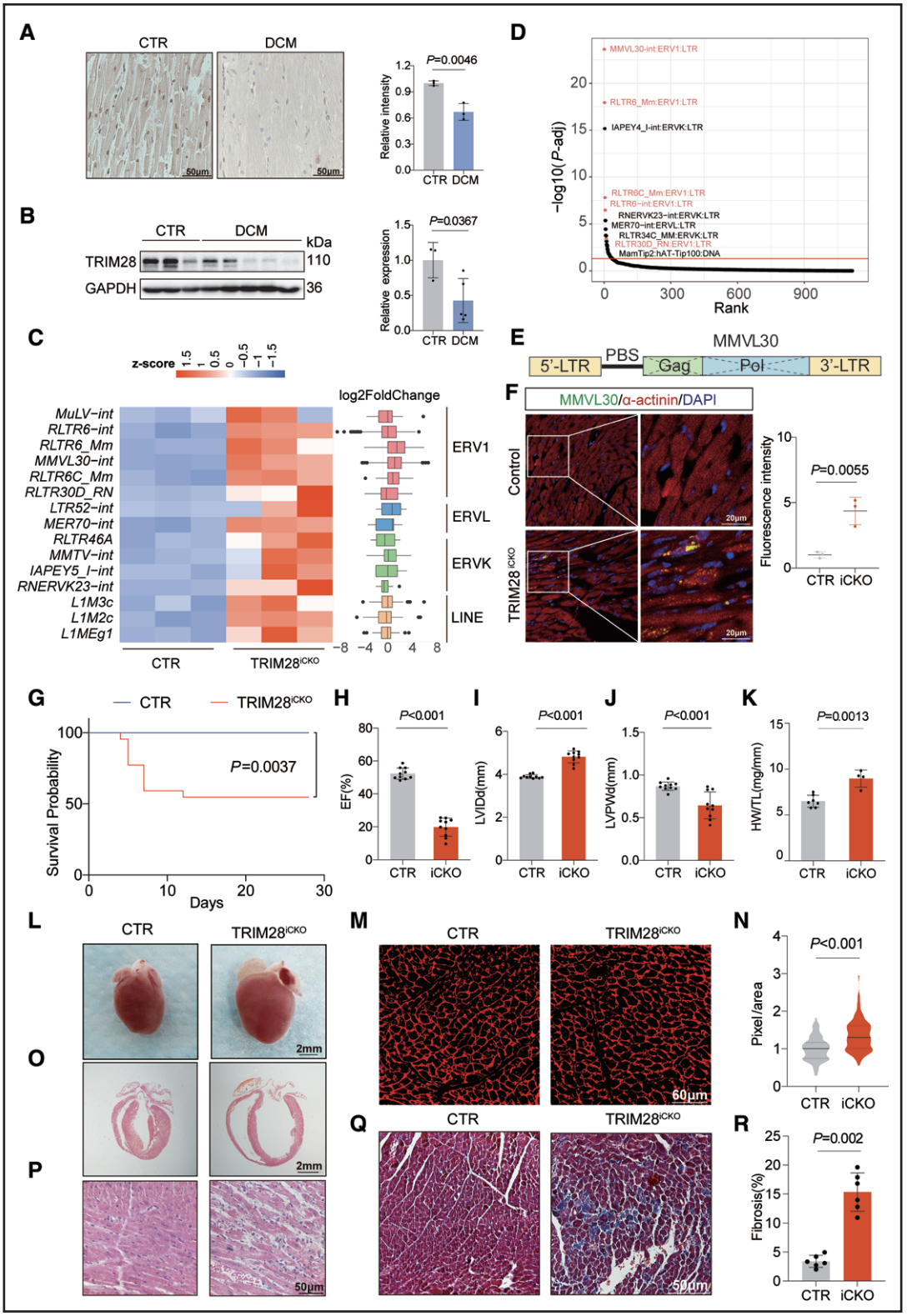

Figure 2. The cardiomyocyte-specific deprivation of TRIM28 led to endogenous retrovirus resurgence and heart failure.
A, Immunohistochemical staining of left ventricles from human nonfailing control (CTR) and dilated cardiomyopathy (DCM) hearts. TRIM28 (tripartite motif–containing protein 28) expression is significantly reduced in human DCM hearts. Quantification of TRIM28-positive nuclei (**right**) was performed using ImageJ. Data represent mean±SD; n=3 hearts per group. Two-tailed Student *t* test. **B**, Western blot analysis of TRIM28 protein in CTR and DCM human left ventricles. TRIM28 signal intensity was quantified using ImageJ. The TRIM28 protein level decreased significantly in human DCM hearts. Data are mean±SD; n=3 CTR and 5 DCM hearts. Two-tailed Student *t* test. **C**, RNA sequencing analysis of endogenous retrovirus expression in Myh6-MerCreMer (CTR) and Myh6-MerCreMer TRIM28$^{f/f}$ (TRIM28^{iCKO}) mouse hearts (*Continued*)

Figure 2 Continued. 1 week after tamoxifen induction, showing endogenous retrovirus resurgence in TRIM28^{iCKO} hearts. RLTR6_Mm and MMVL30-int exhibited the most significant upregulation. **D**, Adjusted *P* value ranking indicated that endogenous retrovirus class 1 exhibited the most significant alterations after TRIM28 depletion. MMVL30-int, RLTR6_Mm, RLTR6-int, RLTR6C_Mm, and RLTR30D_RN of mouse endogenous retrovirus class 1, in red, ranked in the top 10 in differentially expressed RTEs. The red horizontal line indicates adjusted *P*=0.05. **E**, The structure of the MMVL30 provirus in the mouse genome. **F**, RNA fluorescence in situ hybridization detecting the MMVL30 transcripts (green signal) in CTR and TRIM28^{iCKO} cardiomyocytes (red signal). The MMVL30 signal intensity (**left**) was quantified with ImageJ (**right**). Data are mean±SD; n=3 hearts per group. Two-tailed Student *t* test. **G**, The survival plot of CTR (n=18) and TRIM28^{iCKO} (n=22) mice. Ten of 22 (46%) of TRIM28^{iCKO} mice died within 2 weeks after tamoxifen induction. The statistical significance was calculated with a log-rank test. *P*<0.05 indicated significance. **H** through **J**, M-mode echocardiogram illustrating the attenuated ejection fraction (H), increased left ventricle diastolic internal diameter (I), and decreased left ventricular posterior wall thickness at diastole (J) of TRIM28^{CKO} hearts. Data are mean±SD; n=10 mice per group. Two-tailed Student *t* test. **K**, The ratio of heart weight to tibial length in CTR (n=7) and TRIM28^{iCKO} (n=4) mice. Data are mean±SD. Two-tailed Student *t* test. **L**, Gross anatomy showing the significant enlargement of TRIM28^{iCKO} hearts. **M** and **N**, Wheat germ agglutinin staining of left ventricular sections, illustrating the enlarged cardiomyocytes in TRIM28^{iCKO} hearts. The areas of cardiomyocytes (**M**) were calculated with ImageJ (**N**). N=110 to 118 cells from 3 measured hearts per group. Mean±SD, 2-tailed Student *t* test. **O**, Hematoxylin-eosin staining illustrates the dilated cardiomyopathy of TRIM28^{iCKO} hearts. **P,** Hematoxylin-eosin histology showing sarcomere disarrangement, cardiomyocyte death, and inflammatory cell infiltration in TRIM28^{iCKO} hearts. **Q**, Masson trichrome staining showing increased collagen deposition (blue region) in TRIM28^{iCKO} hearts. **R**, The quantification of trichrome staining revealed elevated collagen deposition in TRIM28^{iCKO} hearts. Mean±SD, n=6 mice per group. Two-tailed Student *t* test. EF indicates ejection fraction; ERV, endogenous retrovirus; Gag, group-specific antigen; HW, heart weight; LTR, long terminal repeat; LVIDd, left ventricle diastolic internal diameter; LVPWd, left ventricular posterior wall thickness at diastole; Pol, polyprotein; and TL, tibial length.

CTRL hearts, with increased ratio of heart weight to tibial length and enlargement of individual cardiomyocytes (*P*=0.0013; Figure 2K through 2N). Histology further confirmed the increased chamber size and much thinner myocardial wall of TRIM28^{iCKO} hearts, which were in agreement with the echocardiography results (Figure 2O). Specifically, we observed broken and disarrayed muscle bundles infiltrated with a large amount of blood cells, particularly monocytes, indicating active cell death and inflammation within the myocardium (Figure 2P). Even just 7 days after TRIM28 deletion, significant fibrosis was evident in TRIM28^{iCKO} hearts (Figure 2Q and 2R). Biomarkers of HF, including Nppa (natriuretic peptide A) and Nppb (natriuretic peptide B), were upregulated in TRIM28^{iCKO} hearts, and the adult Myh6 (myosin heavy chain α)/Myh7 (fetal myosin heavy chain 7) ratio was significantly reduced (Figure S3A). Together, these results indicate that TRIM28 deletion in myocardium leads to AHF and severe HF. This AHF caused prominent congestion and edema in the lungs and liver of TRIM28^{iCKO} mice (Figure S3B), resembling clinical manifestations of AHF patients.

TRIM28 Regulated Histone and RNA Methylation to Restrain ERV Resurgence

As a core member of the methyltransferase complex, TRIM28 is crucial in maintaining H3K9 methylation, whereas its depletion might lead to ERV resurgence.[32] To test this hypothesis, we profiled the chromatin occupancy of H3K9me3 around genomic TEs in wild-type and TRIM28^{iCKO} hearts using chromatin immunoprecipitation sequencing (Figure 3A and 3B). The analysis showed that 27.8% ERV RTEs were occupied by H3K9me3 predominantly in the coding region, which decreased in TRIM28^{iCKO} hearts (Figure 3Aa). Among the upERVs containing 1723 transcripts in total, 38.9% of them were significantly occupied by H3K9me3. Of the H3K9me3-targeted upERVs, 59.6% lost their occupancy in TRIM28-deficient hearts, whereas the others either remained unaltered or exhibited increased H3K9me3 occupancy (Figure 3B and 3C). In line with this result, the IGV snapshot showed that H3K9me3 occupancy decreased on the genome of upregulated MMVL30-int_dup726 but not on MMVL30-int_dup810 RTE, which was also elevated in the TRIM28^{iCKO} hearts (Figure 3D and 3E). Together, these results suggest that loss of TRIM28-mediated H3K9me3 only partially contributes to the mechanism of ERV resurgence.

To further investigate this assumption, we generated a transgenic mouse with an inducible deletion of SETDB1 (SETDB1^{iCKO}) in cardiomyocytes. SETDB1 is a methyltransferase of H3K9me3 in complex with TRIM28. Similar to TRIM28^{iCKO} hearts, SETDB1^{iCKO} hearts also showed increased ERV expression, although less pronounced than in TRIM28^{iCKO} hearts (Figure S4A). SETDB1^{iCKO} mice had impaired systolic functions and DCM 7 days after tamoxifen induction, which was characterized by both an increased internal diameter and reduced posterior wall of the left ventricle at end diastole, as measured by echocardiography. These changes in SETDB1^{iCKO} mice were similar but milder when compared with those observed in TRIM28^{iCKO} mice (CTR versus SETDB1^{iCKO} hearts, ejection fraction: 54.53±2.28 versus 30.11±4.97, *P*<0.001; fractional shortening: 27.79±1.43 versus 14.12±2.54, *P*<0.001; left ventricular end-diastolic internal diameter: 3.88±0.15 versus 4.64±0.35, P=0.0019; left ventricular end-diastolic posterior wall thickness: 0.85±0.09 versus 0.63±0.0, *P*<0.001; Figure S4B through S4E; Table S5). Postmortem examination further confirmed these heart phenotypes showing consistent but less severe DCM (Figure S4F). In agreement with the phenotype, all SETDB1^{iCKO} mice survived up to 1 month after tamoxifen induction, in sharp contrast with TRIM28^{iCKO} mice, whereas 46% died 2 weeks after tamoxifen induction (Figure S4G). These results support our hypothesis that

ORIGINAL RESEARCH ARTICLE

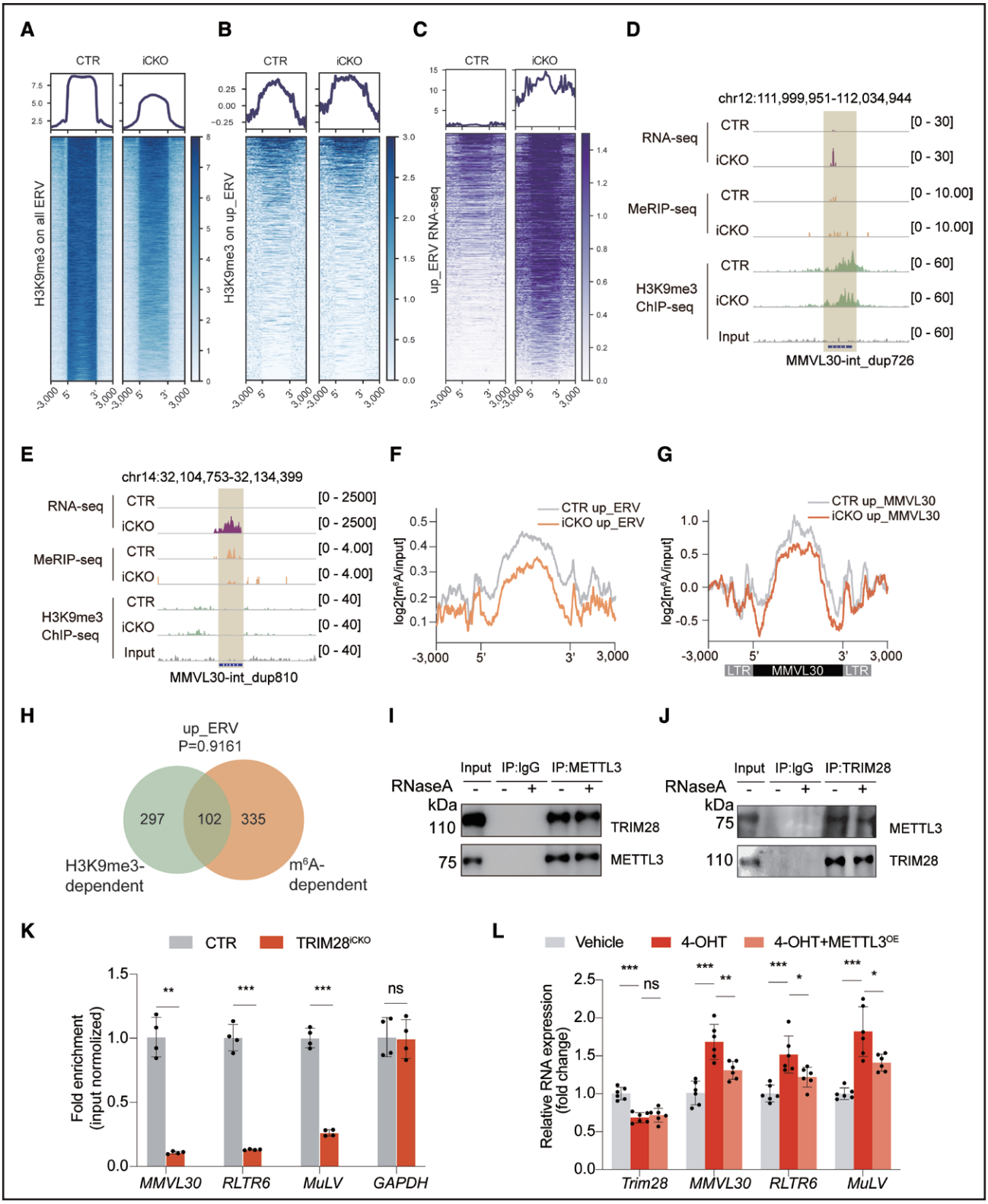

Figure 3. TRIM28 controlled the surveillance of endogenous retrovirus class 1 by manipulating trimethylation at lysine 9 of histone H3 and N6-methyladenosine.

A, Trimethylation at lysine 9 of histone H3 (H3K9me3) chromatin immunoprecipitation sequencing signals on all targeted endogenous retroviruses (ERVs). **B**, H3K9me3 chromatin immunoprecipitation sequencing signals on upregulated ERVs. **C**, RNA sequencing heatmap of those upregulated ERVs. **D**, H3K9me3, RNA, and methylated RNA immunoprecipitation sequencing signals on upregulated MMVL30-int_dup726 RTE genomic loci, illustrating the declined H3K9me3 and intact *N*^{6}-methyladenosine (m^{6}A). **E**, H3K9me3, RNA sequencing, and methylated RNA immunoprecipitation sequencing signals on the upregulated MMVL30-int_dup810 transcript, illustrating the increased m^{6}A and (*Continued*)

Figure 3 Continued. unchanged H3K9me3. **F**, Aggregation plot showing that the average m^{6}A signal was lower on upregulated ERVs in TRIM28^{iCKO} hearts. **G**, Aggregation plot showing that the average m^{6}A signal was downregulated on up_MMVL30 RTE transcripts in TRIM28^{iCKO} hearts. Shown beneath the aggregation plot is the genomic structure of MMVL30. **H**, Venn diagram showing the minimal overlap between m^{6}A- and H3K9me3-modulated upregulated ERVs. Only 23% (102 of 437) of m^{6}A-modified upregulated ERVs were also marked by H3K9me3. *P*=0.9161 by χ^2 test. **I** and **J**, Immunoprecipitation revealed the interactions between TRIM28 (tripartite motif–containing protein 28) and METTL3. **K**, RIP-qPCR revealed that the binding of METTL3 to ERVs decreased in TRIM28^{iCKO} hearts. GAPDH served as a negative control. Mean±SD, n=4; ***P*<0.01, ****P*<0.001; 2-tailed Student *t* test. **L**, RT-qPCR revealed that METTL3 overexpression suppressed ERV activation in TRIM28^{iCKO} CM. Mean±SD, n=6, 2-tailed Student *t* test; **P*<0.05, ***P*<0.01, ****P*<0.001. ChIP-seq indicates chromatin immunoprecipitation sequencing; MeRIP-seq, methylated RNA immunoprecipitation sequencing; ns, no significance; RNA-seq, RNA sequencing; and RT-qPCR, reverse transcription-quantitative polymerase chain reaction.

H3K9me3 modification is only partially responsible for ERV activation and ERV-induced HF.

RNA methylation, specifically m^{6}A, can prompt RNA decay, including RTEs. The resurgence of H3K9me3-unregulated upERVs might result from the alteration of m^{6}A modification.[33] Thus, we profiled m^{6}A modification by methylated RNA immunoprecipitation sequencing and identified 11 300 peaks in wild-type and 9612 m^{6}A peaks in TRIM28^{iCKO} hearts (Figure S5A). m^{6}A was highly enriched both at 3′ and 5′ UTRs of protein-coding mRNA, as reported for other cells,[34] and there was no significant difference observed between wild-type and TRIM28^{iCKO} hearts (Figure S5B). In contrast, there was a notable reduction of m^{6}A within the internal regions of upERVs, such as MMVL30, after TRIM28 depletion (Figure 3E through 3G). Some upERV RTEs, such as MMVL30-int_dup810, MuLV-int_dup62, and RLTR6-int_dup581, had decreased m^{6}A but no detectable signals or changes in H3K9me3 on their genome, suggesting that m^{6}A plays an H3K9me3-independent role in ERV activation (Figure 3E; Figure S5C). This conclusion was further supported by a gene overlap assay showing that m^{6}A-modified upERVs were largely distinct from those marked by H3K9me3 (1723 transcripts, *P*=0.9161; Figure 3H). To better understand the molecular mechanism, we performed the reciprocal immunoprecipitation and found that TRIM28 interacts with METTL3, an enzymatic writer of m^{6}A,[35] which was independent of RNA (Figure 3I and 3J). The RNA immunoprecipitation assay showed that TRIM28 deficiency dampened METTL3 binding to the upERVs, such as MMVL30, RLTR6, and MuLV (Figure 3K). Conversely, overexpressing METTL3 in TRIM28^{iCKO} cardiomyocytes attenuated the upregulation of these upERVs (Figure 3L). Together, these results imply that TRIM28 simultaneously regulates H3K9me3 and RNA methylation to maintain the silence of ERVs. Interrupting this surveillance mechanism can lead to ERV resurgence in HF.

ERV Resurgence Induced Innate Inflammation and Myocarditis

To investigate a possible role of ERV activation in HF pathogenesis, we analyzed the mRNA transcriptome in TRIM28^{iCKO} hearts by RNA-seq. Principal component analysis indicated that the transcriptomes in wild-type and TRIM28^{iCKO} hearts were largely distinct (Figure S6A). A total of 6311 genes were differentially expressed, including 2894 genes downregulated and 3417 upregulated (fold change>1.5, *P*-adj<0.05; Figure S6B). Gene Ontology analysis revealed that, among the upregulated differentially expressed genes, inflammation-related terms were dominant among the top enriched terms, with *P*-adj<9.75e−19, indicating prominent immune activation (the top 10 ranking terms are listed in Figure 4A). For the downregulated differentially expressed genes, the energetic and metabolic terms were enriched, further confirming the HF phenotype of TRIM28^{iCKO} hearts (Figure S6C). To further identify which immune pathway was activated in TRIM28-deficient hearts, we implemented gene set enrichment analysis, which illustrated significant enrichments of TLR signaling and cytosolic DNA sensing, the pathways related to the pattern recognition receptor and innate immunity[10] (Figure 4B and 4C). We also detected double-stranded RNA, a canonical immunogen for antivirus and innate immunity, which further supported the activation of innate immunity in TRIM28^{iCKO} cardiomyocytes (Figure S6D and S6E). The NF-κB and IFN I pathways are the 2 canonical pathways downstream of pattern recognition receptor activation.[36] Intriguingly, gene set enrichment analysis revealed that NF-κB, rather than the IFN I pathway, was activated upon TRIM28 deletion, which implied a unique activation pattern of innate immunity in TRIM28^{iCKO} hearts (Figure 4D and 4E).

To further dissect the pattern recognition receptor pathways related to innate immunity, we first examined the protein levels of several key components. We observed a substantial increase in TLR7 (a TLR-detecting single-stranded RNA), TLR9 (a TLR-detecting unmethylated CpG-containing single-stranded DNA), MyD88 (a key signaling transduction adaptor downstream of TLRs forming the supramolecular organizing center myddosome), and cGMP-AMP (cGAS; a sensor for cytosolic DNA),[10,36] in TRIM28^{iCKO} hearts (Figure 4F and 4G; Figure S6F). Additionally, we observed a notable increase in the phosphorylation of P65 and TAK1, an upstream kinase for P65, indicating activation of the NF-κB pathway. By contrast, phosphorylation of the transcription factor IRF7, a key regulator of type I IFN gene expression, remained unchanged, which was in line with the gene set enrichment analysis showing no change of the

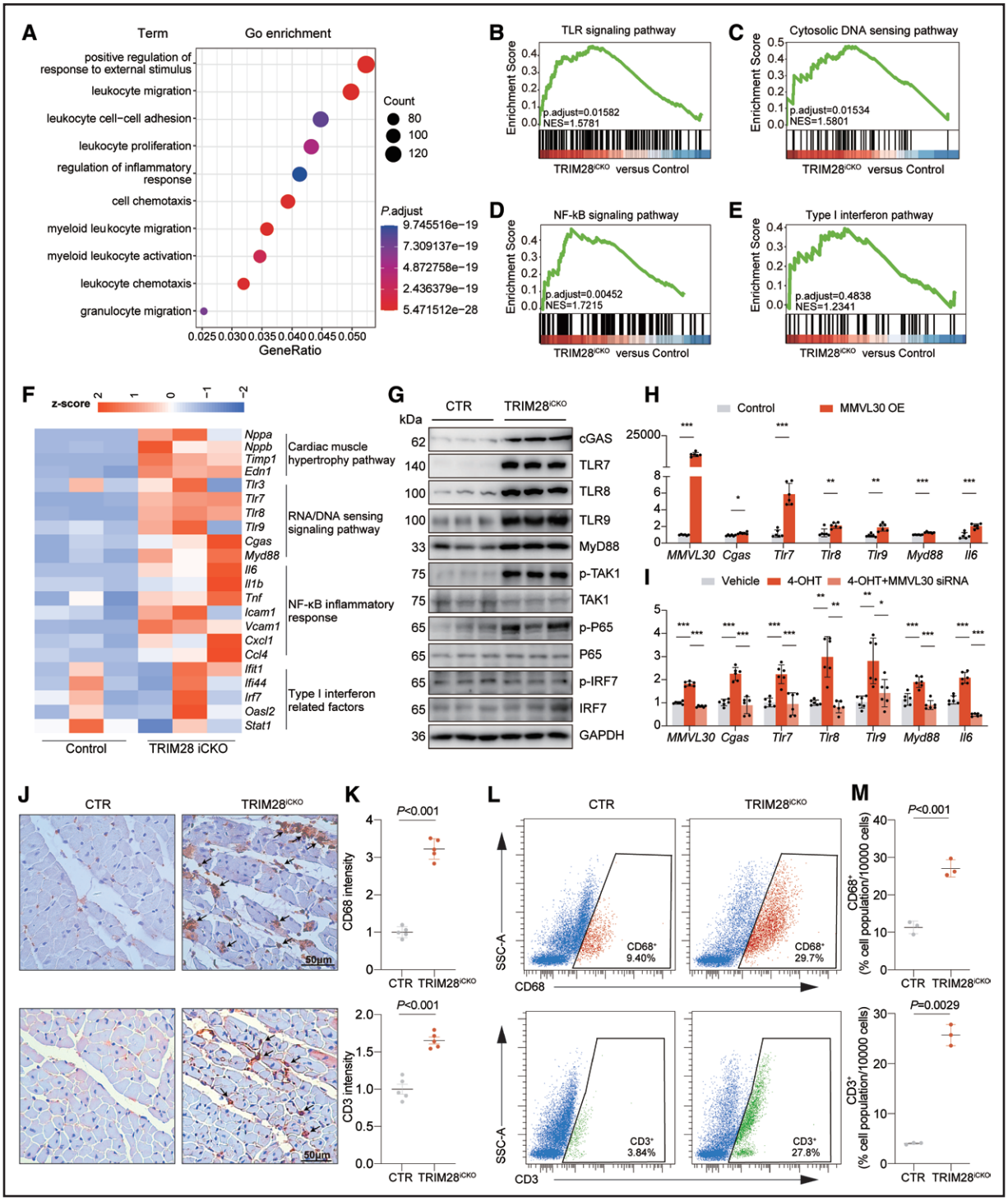

Figure 4. Endogenous retrovirus resurgence leads to myocarditis and heart failure through activation of TLR7/9.
A, Gene Ontology analysis of upDEGs. The top 10 enriched terms are shown. The color scale indicates the adjusted *P* value (*P*-adjust). **B** through **E**, Gene set enrichment analysis analyzing the gene enrichment in nucleic acid–sensing pathways of TLR (Toll-like receptor; **B**), cGMP-AMP (cGAS; **C**), NF-κB (**D**), and IFN (interferon; **E**). Significant enrichments were observed in TLR (normalized enrichment score [NES]=1.5781; *P*-adjust<0.05), cGAS (NES=1.5801; *P*-adjust<0.05), and NF-κB (NES=1.7215; *P*-adjust<0.01) pathways but not IFN (NES=1.2341; *P*-adjust=0.4838). **F**, Heatmap showing differentially expressed genes in the cardiac hypertrophy, nucleotide sensing, and NF-κB pathways. Genes in the IFN pathway were not significantly altered. **G**, Western blot illustrating the activation of the PRR (pattern recognition receptor; including cGAS, TLR7, TLR8, TLR9, MyD88, TAK1, and p-TAK1) and NF-κB (p-P65 and P65) pathways but not IFN (p-IRF7 and IRF7) in TRIM28^{iCKO} hearts. GAPDH served as a control. **H**, RT-qPCR examination of TLR7/9 and cGAS activation in primary cardiomyocytes transduced with MMVL30. Data were normalized to GAPDH. Mean±SD, n=6 independent replicates, 2-tailed Student *t* test; **P*<0.05, ***P*<0.01, ****P*<0.001. **I**, RT-qPCR indicated that MMVL30 siRNA suppressed TLR7/9 and cGAS pathway activation in TRIM28 (tripartite motif–containing protein 28) knockout cardiomyocytes. Primary cardiomyocytes were treated with 4-hydroxytamoxifen to induce TRIM28 deletion and (*Continued*)

Figure 4 Continued. then transfected with METTL3-modified RNA for 48 hours. Mean±SD, n=6 independent replicates. One-way ANOVA followed by post hoc Tukey test. *P<0.05, **P<0.01, ***P<0.001. **J** and **K**, Immunochemistry revealing the infiltration of CD68+ macrophages (**J**, **top**) and CD3+ lymphocytes (**J**, **bottom**). Arrows indicate infiltrated immune cells. The intensity of CD68+ macrophages (**K**, **top**) and CD3+ lymphocytes (**K**, **bottom**) was calculated with ImageJ. Data are mean±SD, n=5 hearts. Two-tailed Student *t* test. **L** and **M**, Flow cytometry demonstrating increased CD68+ macrophages and CD3+ lymphocytes in TRIM28^{iCKO} mice (**L**). The numbers of CD68+ macrophages (**M**, **top**) and CD3+ lymphocytes (**M**, **bottom**) were calculated in FlowJo. Mean±SD, n=3 mice, Two-tailed Student *t* test. 4-OHT indicates 4-hydroxytamoxifen; FDR, false discovery rate; GO, Gene Ontology; and RT-qPCR, reverse transcription-quantitative polymerase chain reaction.

IFN pathway (Figure 4G). Consistently, the inflammatory cytokines IL6, IL1b, TNFα, VCAM1, and ICAM1, all downstream of NF-κB, were significantly increased, whereas IFN-stimulated genes such as IFIT1 and IFI44 remained unchanged (IFIT1: *P*-adj=0.62; IFI44: *P*-adj=0.91; Figure 4F; Figure S6G).

MMVL30 in the ERV1 category is unable to form viral particles because of the multiple stop codons embedded in its coding region. However, the RNA/DNA transcribed from MMVL30 can still activate the innate immune response and cause pathogenesis.[28] To further examine whether the innate immune response is linked to ERV resurgence, we overexpressed MMVL30 RNA in cardiomyocytes using modified RNA and found that TLR7/9, MyD88, and cGAS were robustly induced (Figure 4H). Conversely, using siRNA to suppress the MMVL30 induced in TRIM28^{iCKO} cardiomyocytes attenuated the activation of TLR7/9, MyD88, and cGAS (Figure 4I). Both findings support the theory that the resurgence of ERV RNA induces innate immune activation in TRIM28^{iCKO} myocardium. This aberrant innate immune activation subsequently triggered adaptive cellular immunity and myocarditis, characterized by elevated infiltration of CD3+ lymphocytes and CD68+ macrophages in the myocardium (Figure 4J through 4M), which further caused cell death, as evidenced by the increased release of LDH in the serum (Figure S7A). Time-series experiments also supported this observation, showing a simultaneous increase in ERV and inflammatory gene expression in TRIM28^{iCKO} hearts, which occurred before the expression of HF-related genes (Figure S7B). This sequence of events highlights the role of aberrant ERV resurgence in initiating the innate immune response, which subsequently contributes to myocarditis and HF.

ERVs Induced Myocarditis via the TLR7/9–NF-κB Pathway

Based on the observation of activation of the antivirus and exogenous nucleotide pathways TLR7/9 and cGAS in response to ERV resurgence, we continued to dissect their functional roles in ERV-mediated myocarditis and HF. We treated TRIM28^{iCKO} mice with the cGAS-STING inhibitor C176, the TLR7/9 inhibitor NSC4375, or the NF-κB inhibitor JSH23 for 21 days (Figure 5A) and evaluated heart function with echocardiography and histology assays. To further validate the role of ERVs in myocarditis and HF in vivo, we also treated TRIM28^{iCKO} mice with the reverse transcriptase inhibitor (RTi) zidovudine to suppress ERV reverse transcription and immunogenicity. Treatments with JSH23, NSC4375, and RTi for 3 weeks increased the survival of TRIM28^{iCKO} mice, whereas C176 treatment did not yield a significant improvement (Figure 5B; JSH23: 85.7%, *P*=0.013; NSC4375: 79.2%, *P*=0.041; RTi: 80.9%, *P*=0.032; C176: 62.5%, *P*=0.619 versus TRIM28^{iCKO}: 53.8%). Congruently, JSH23, NSC4375, and the RTi significantly improved the systolic function of TRIM28^{iCKO} hearts and alleviated DCM (Figure 5C through 5H; Table S5). Although C176 showed a trend toward improving heart function and mitigating remodeling, the effects were not statistically significant. In addition, JSH23 and NSC4375 markedly reduced macrophage infiltration and cytokine expression without affecting ERV levels, suggesting that these 2 compounds attenuated the HF phenotype through inhibition of TLR7/9 and NF-κB, which is downstream of ERV resurgence (Figure 5I; Figure S8A through S8C). Similarly, RTi did not affect ERV expression but profoundly suppressed cytokine elevation and macrophage infiltration, confirming the role of ERVs in driving immune activation and myocarditis in TRIM28^{iCKO} hearts (Figure 5I; Figure S8A through S8C). In contrast, C176 had no significant effects on ERV expression or inflammatory responses, further excluding a role of the cGAS pathway in ERV-mediated innate immunity and HF. Collectively, these results define a critical role of the TLR7/9–NF-κB axis as the downstream signaling transduction pathway responsible for ERV resurgence-induced myocarditis and HF.

Constraining ERV Resurgence Alleviated HF in an I/R Model

Percutaneous coronary intervention, a widely used clinical procedure, often causes I/R injury, leading to acute cardiac inflammation and HF. Next, we examined ERV resurgence using a mouse I/R model. We observed downregulation of TRIM28 and SETDB1, accompanied by robust activation of ERVs, particularly ERV1, including MMVL30, in I/R mouse hearts (Figure 6A; Figure S9A). Upregulation of ERV1 and cytokines (IL6, IL1b, and TNFα) occurred immediately after surgery, before induction of the HF marker Nppa, which indicated that ERV functioned as a driving factor in the I/R HF model (Figure 6A). Western blot and RNA-seq analysis further confirmed the downregulation of TRIM28 and activation of the TLR7/9–NF-κB pathway in I/R hearts (Figure 6B; Figure S9B). These results were in agreement with those

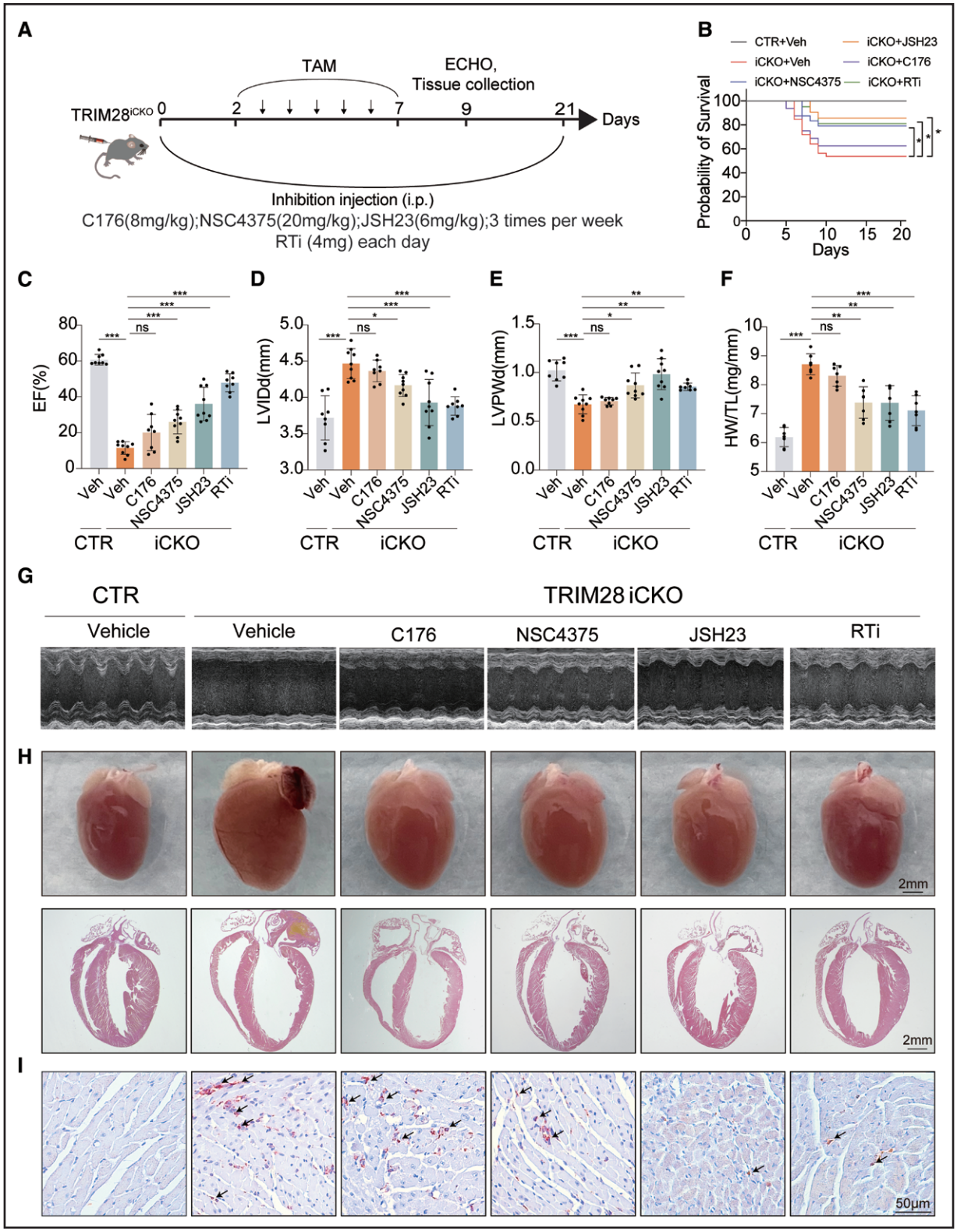

Figure 5. Blocking the endogenous retrovirus–Toll-like receptor–NF-κB pathway ameliorated myocarditis and cardiac dysfunction of TRIM28^{iCKO} mice.

A, Dosing strategies of variable small-molecule inhibitors. NSC4375 (a TLR7/9 [Toll-like receptor 7/9] inhibitor, 20 mg/kg), JSH23 (an NF-κB inhibitor, 6 mg/kg), and C176 (a cGMP-AMP inhibitor, 8 mg/kg) as well as vehicle (5% DMSO+40% PEG300+5% Tween 80+50% ddH_2O) were administered via intraperitoneal injection 3 times per week. The reverse transcriptase inhibitor (RTi; zidovudine, 4 mg/day) was dosed via drinking water. Mice were subsequently evaluated with ECHO and pathology. **B**, The survival of TRIM28^{iCKO} mice with or without inhibitor treatments. Treatments with NSC4375, JSH23, or RTi for 3 weeks increased the survival of TRIM28^{iCKO} mice. (*Continued*)

Figure 5 Continued. The statistical significance was calculated with log-rank tests. $P<0.05$ indicated significance. **C** through **E**, Echocardiogram revealed that NSC4375, JSH23, and RTi significantly alleviated the pathological remodeling of TRIM28^{iCKO} hearts. NSC4375, JSH23, and RTi rather than C176 improved the systolic function of TRIM28^{iCKO} mice (**C**), decreased the left ventricle diastolic internal diameter (D) and increased the left ventricular posterior wall thickness at diastole (**E**). Mean±SD, n=8 to 9 mice, 1-way ANOVA followed by post hoc Tukey test; *$P<0.05$, **$P<0.01$, ***$P<0.001$. **F**, Heart weight/tibial length ratio verified that NSC4375, JSH-23, and RTi rather than C176 reduced the heart mass of TRIM28^{iCKO} mice. Mean±SD; n=7 mice; 1-way ANOVA followed by post hoc Tukey test. **$P<0.01$, ***$P<0.001$. **G**, The M-mode echocardiograms of TRIM28^{iCKO} mice 9 days after inhibitor treatments. NSC4375, JSH23, and RTi improved cardiac function. **H**, The gross anatomy (**top**) and hematoxylin-eosin staining sections (**bottom**) revealed that NSC4375, RTi, and JSH23 ameliorated the ventricular dilation of TRIM28^{iCKO} hearts. **I**, Immunohistochemistry revealed that NSC4375, JSH23, and RTi mitigated the infiltration of CD68^{+} macrophages. Arrows indicate infiltrating CD68^{+} macrophages. CD68^{+} macrophages in hearts are quantified in Figure S8C. HW indicates heart weight; LVIDd, left ventricle diastolic internal diameter; LVPWd, left ventricular posterior wall thickness at diastole; ns, no significance; and TL, tibial length.

in TRIM28^{iCKO} hearts, indicating a potential role of the ERV–TLR7/9–NF-κB axis in ischemic HF.

To further support this hypothesis, we also used a gain-of-function approach. We engineered AAV9 expressing TRIM28 under the control of a cardiac-specific troponin T promoter and administered 2.5×10^{11} vg viruses through an intrathoracic injection 7 days before I/R surgery for sustained TRIM28 expression in myocardium during I/R (Figure S9C). TRIM28 reintroduction substantially suppressed the activation of ERVs, further supporting the role of TRIM28 in silencing ERVs (Figure 2 and Figure 6C). Moreover, AAV9-TRIM28 attenuated activation of the TLR7/9–NF-κB pathway and the expression of IL6, IL1b, and TNFα (Figure 6B and 6C). AAV9-TRIM28 also reduced myocardial damage and cell death, as shown by reduced serum LDH (Figure S9D). These results indicate that AAV9-TRIM28 is able to suppress ERV resurgence and inflammatory response in the I/R model.

Next, we evaluated whether AAV9-TRIM28 could preserve cardiac function after I/R. Perfusion with Evans blue 24 hours after I/R surgery was used to evaluate the extent of ischemia and the injured area, which showed that AAV9-TRIM28 did not alter the area at risk but significantly reduced the infarct region/area at risk, the area of I/R-induced myocardial injury (Figure 6D through 6F, from 41.5% to 31.6% ($P=0.0024$). Time-series echocardiography demonstrated a significant improvement of systolic function as early as 24 hours, which was sustained up to 3 weeks after I/R induced by AAV-TRIM28 treatment (Figure 6G; Table S5). AAV9-TRIM28 also decreased scar size at the end point of 3 weeks after I/R (Figure 6H and 6I; I/R+CTR versus I/R+TRIM28, from 14.5% to 7.9%, $P<0.001$). These results collectively imply that AAV9-mediated TRIM28 expression effectively suppresses ERV activation to protect against HF.

Intercepting ERV-Mediated Innate Immunity Alleviated HF in the I/R Model

The detection of TLR7/9 and NF-κB activation indicated active ERV-mediated innate immunity in the I/R model (Figure 6A). Therefore, we further examined its functional role in I/R-induced cardiac inflammation and dysfunction. Treatment with 20 mg/kg NSC4375 in I/R mice, which is the same dose as used in TRIM28^{iCKO} mice 2 days before I/R (Figure 7A) abolished activation of the MyD88 and NF-κB pathway, as indicated by reduced TAK1 and P65 phosphorylation (Figure 7B). NSC4375 also suppressed the expression of cytokines (IL6, IL1b, and TNFa) but not ERVs (MMVL30, RLTR6, and MuLV), further confirming the signaling cascade and the functional role of the ERV–TLR7/9–NF-κB molecular axis in I/R (Figure 7C). In agreement with the results observed with AAV-TRIM28, NSC4375 substantially decreased the infarct size of I/R hearts (Figure 7D through 7F) from 43.5% to 36.6% ($P=0.035$) and improved the contractile function (Figure 7G; Table S5). As expected, NSC4375 also markedly reduced scar size from 12.2% to 5.7% (Figure 7H and 7I; $P=0.0052$). In summary, these results illustrate that activation of the ERV–TLR7/9–NF-κB axis exacerbates cardiac dysfunction in the I/R model and that intercepting its activation effectively alleviates inflammation and HF induced by I/R.

DISCUSSION

In summary, our study provides the first evidence showing that the resurgence of ERVs, particularly ERV1, is a unique trait of multiple types of HF. We identified that the aberrant ERV expression in cardiomyocytes, driven by TRIM28 depletion, acts as a novel immunogen to induce myocardial inflammation, cell death, and AHF through the TLR7/9–NF-κB pathway (Figure S10). Our results established a new pathogenic axis of TRIM28–ERV–TLR–NF-κB, which plays a critical role in myocarditis and HF. Targeting this axis effectively protects against myocarditis and ischemic HF.

Recent studies have indicated that RTEs play critical roles in several essential biological processes, such as embryogenesis,[8,18] aging,[37] and neurodegenerative disorders.[8–10,23,26] However, before this study, the possible involvement and pathogenic mechanisms of ERV resurgence in HF remain unexplored. Here, we show that LTR ERVs, particularly the ERV1 subclass, are consistently activated in diverse types of HF, including DCM, myocardial infarction, and I/R, across multiple species, including humans, nonhuman primates, and rodents, whereas the non-LTR RTEs LINEs and SINEs are not. There

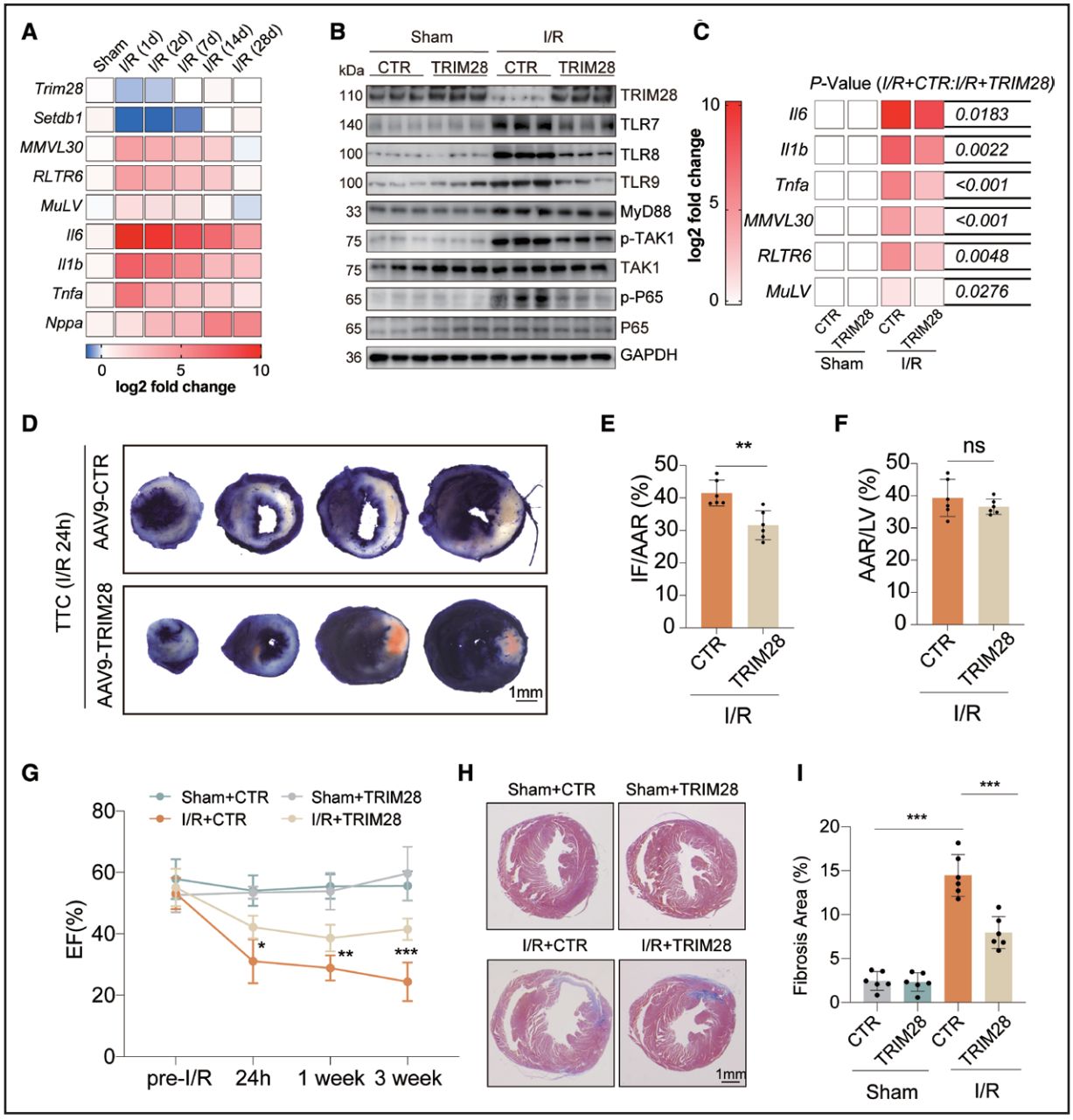

Figure 6. Curbing endogenous retrovirus resurgence mitigates heart failure.
A, Heatmap of RT-qPCR showing the time-course expression profiling in the ischemia/reperfusion mouse model. TRIM28 (tripartite motif–containing protein 28) and SETDB1 were significantly downregulated, whereas endogenous retroviruses and cytokines were activated immediately after surgery, which was ahead of Nppa (natriuretic peptide A). Mean, n=4. **B**, Western blot showing that adeno-associated virus serotype 9 (AAV9)-TRIM28 inhibited activation of the TLR7/9 (Toll-like receptor 7/9) and NF-κB pathways in ischemia/reperfusion hearts. **C**, AAV9-TRIM28 suppressed endogenous retrovirus class 1 and cytokine expression in the ischemia/reperfusion hearts, as revealed by reverse transcription-quantitative polymerase chain reaction. n=6. Mean±SD, 2-way ANOVA followed by post hoc Sidak test. **D**, Evans blue/triphenyl-2H-tetrazolium chloride staining illustrating that AAV9-TRIM28 reduced the infarct area. Blue, nonischemic region; red, ischemic region or area at risk; white, infarct region. **E** and **F**, The calculation of the infarct area. The infarct areas (infarction/area at risk) of AAV9-TRIM28–treated hearts were smaller than those of control hearts. n=6 mice, mean±SD, 2-tailed Student *t* test, ***P*<0.01. **G**, Echocardiography indicating that AAV9-TRIM28 significantly improved the systolic function of ischemia/reperfusion hearts. Ejection fraction was measured for 3 consecutive weeks. n=8 mice. Mean±SD, mixed-effects ANOVA with post hoc Sidak test. **P*<0.05, ***P*<0.01, ****P*<0.001. **H** and **I**, Masson trichrome staining showing that AAV9-TRIM28 ameliorated scar formation 3 weeks after injection. The ratio of fibrotic region (blue) to total region (blue+red) was calculated by ImageJ. n=6 mice. Mean±SD, 2-way ANOVA followed by post hoc Sidak test. ****P*<0.001. AAR indicates area at risk; EF, ejection fraction; IF, infarction; I/R, ischemia/reperfusion; LV, left ventricle; ns, no significance; RT-qPCR, reverse transcription-quantitative polymerase chain reaction; and TTC, triphenyl-2H-tetrazolium chloride.

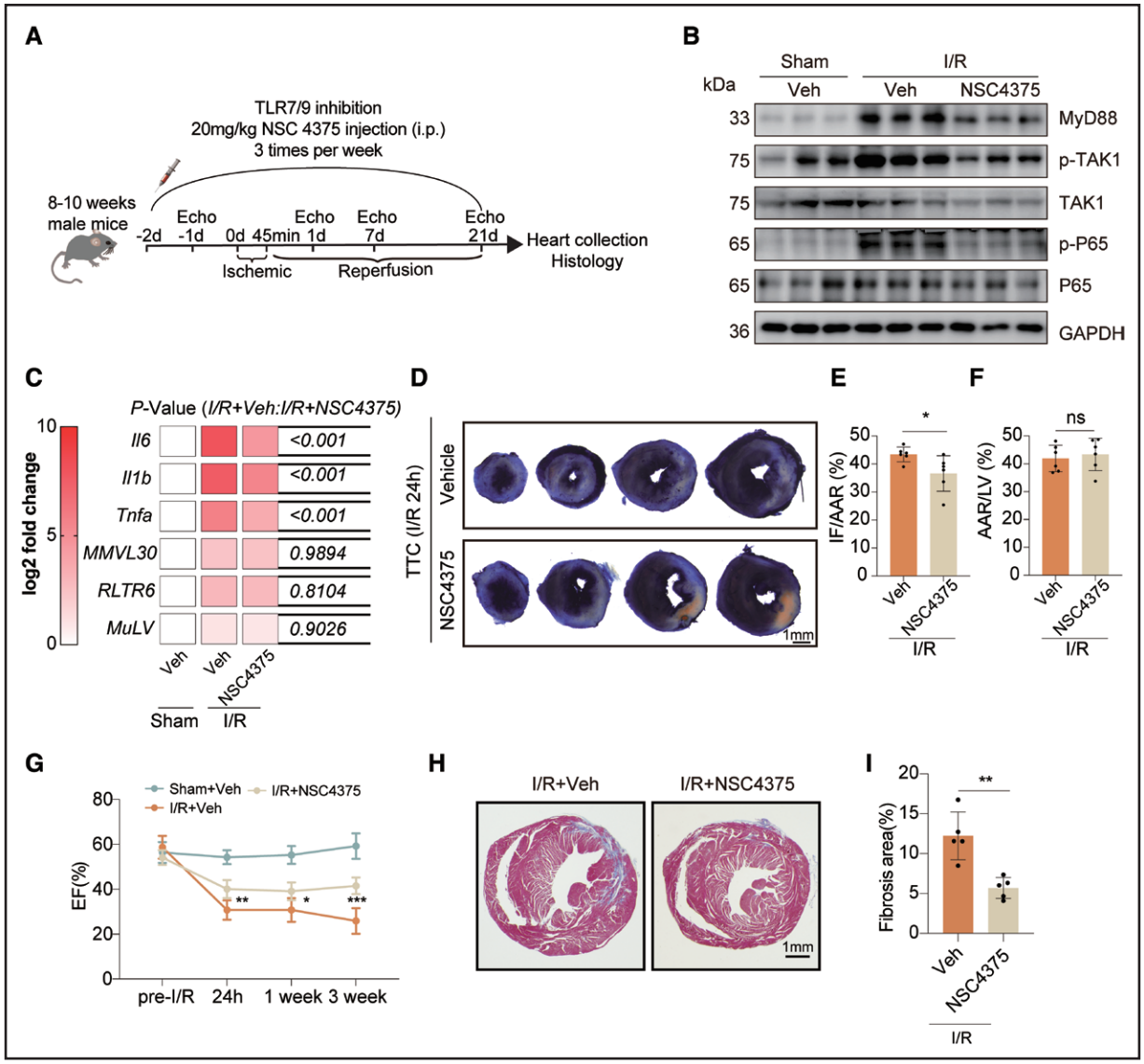

Figure 7. Repressing endogenous retrovirus–mediated innate inflammation mitigates heart failure.
A, NSC4375 dosing strategy: 20 mg/kg of NSC4375 injected intraperitoneally 3 times per week 2 days before ischemia/reperfusion (I/R) surgery. Serial echocardiography was performed at the relevant times, and hearts were collected for pathological analysis 3 weeks after I/R surgery. **B**, Western blot illustrating that NSC4375 suppressed activation of the TLR7/9 (Toll-like receptor 7/9) and NF-κB pathways in I/R hearts. **C**, RT-qPCR showed that NSC4375 suppressed the activation of cytokines (Il6, Il1b, and Tnfa) rather than endogenous retrovirus class 1 (MMVL30, RLTR6, and MuLV) in I/R hearts (I/R+NSC4375 vs I/R+Veh). Mean±SD, n=6, 1-way ANOVA followed by post hoc Tukey test. **D**, Evans blue/triphenyl-2H-tetrazolium chloride staining showing the reduced infarct area in NSC4375-treated I/R mice. **E** and **F**, Calculating the infarct area. The infarct areas (infarction/area at risk) were smaller in NSC4375-treated hearts than in controls (**E**), whereas area at risk/left ventricle remained unchanged (**F**). n= 6 mice, mean±SD, 2-tailed Student *t* test, **P*<0.05. **G**, Echocardiography showing that NSC4375 significantly improved the systolic function of I/R hearts. Ejection fraction was measured for 3 consecutive weeks. Mean±SD, n=8 mice. Mixed-effects ANOVA with post hoc Sidak test. **P*<0.05, ***P*<0.01, ****P*<0.001. **H** and **I**, Trichrome staining revealed that NSC4375 reduced the fibrosis in I/R hearts. Fibrosis was revealed by Masson trichrome staining (**H**) and quantified (**I**) 3 weeks post I/R. Mean±SD, n=5 hearts, 2-tailed Student *t* test, ***P*<0.01. AAR indicates area at risk; EF, ejection fraction; IF, infarction; LV, left ventricle; ns, no significance; RT-qPCR, reverse transcription-quantitative polymerase chain reaction; and TTC, triphenyl-2H-tetrazolium chloride.

are multiple mechanisms identified to suppress RTEs, including histone methylation, DNA methylation, and RNA methylation.[7] In contrast to what we found, ERVs are silenced by H3K9me3 and RNA methylation, LINEs and SINE are mainly silenced by DNA methylation.[10] In agreement, the activation of LINEs and SINEs is often observed in early embryonic development and cancer, in which DNA methylation is rigorously altered.[5,38] Therefore, we reason that the lack of differences of LINEs and SINEs in HF hearts may be attributable to the distinctive silencing mechanism in cardiomyocytes.

Human HERV1 is the second-largest subfamily in LTR-RTEs, comprises nearly 112 000 copies, and occupies 79.2 Mb in the human genome.[39] Among the

9 subgroups of HERV1, HERV-H and HERV-W have been reported to be associated with the pathogenesis of Alzheimer's disease, oncogenesis, and inflammatory disorders.[23,24] However, the HF-associated HERV1 discovered in our study is distinct from HERV-H and HERV-W, belonging to the HEPSI subgroup, and has not been reported in these pathologies, which highlights the specificity and uniqueness of ERV activation in HF. Moreover, in the rodent I/R HF model, ERV1, especially its subfamilies MMVL30-int and RLTR6_Mm, showed the strongest reactivation, further supporting this notion. The distinct trait of HF-associated ERV implicates its potential as a biomarker for clinical diagnosis or prognosis because it can be secreted and, thus, is detectable in the peripheral blood. Of note, the activation of ERVK, but not ERV1, was mainly identified in human HF samples in a meta-RNA-seq analysis.[22] This discrepancy could arise from the difference in detection pipelines, transcript structures, expression threshold, or data sets selected. In the study by Heckmann et al,[22] 23 types of viruses were significantly altered, and 4 of them were retroviruses: the human ERV K113 complete genome, Moloney murine leukemia virus, murine type C retrovirus, and preXMRV-1 provirus. Among them, the Moloney murine leukemia virus and murine type C retrovirus, belonging to the gamma retrovirus family, are the ancestors of ERV1 and share sequence similarities with ERV1. These results together suggest that, although divergent mapping pipelines are used, ERV1 or ERV1-associated virus families are, in fact, activated and detectable in HF hearts. Altogether, these lines of evidence suggest that ERV resurgence could be a universal hallmark of HF, but it requires further validation in broader data sets.

In variable human and animal HF models, ERV1 reactivation is the most pronounced. ERV1 is evolutionarily old, heavily mutated, and lacks the ability to produce the living virus like ERVK.[7] Overexpression of ERV1 RNA transcript MMVL30 in isolated CM activates immunoreaction, whereas knockdown of MMVL30 inhibits inflammation. In addition, suppressing ERV reverse transcription in TRIM28^{iCKO} mice or inhibiting ERV RNA transcription with AAV-TRIM28 in I/R hearts significantly alleviated the inflammatory response and HF. On the contrary, ERVK is evolutionarily young and can generate living viral particles.[10] In our assays, ERVK RNA is not consistently and significantly elevated in human and rodent HF hearts as is ERV1. The amount of ERVK virus envelop in HF hearts is low and not different from CTRL hearts. All of these results allow us to conclude that the activation of ERV RNA transcripts or DNA derives rather than the living virus induce myocarditis and HF directly. In agreement, other studies have also demonstrated that ERV RNA transcripts are able to induce a variety of immune disorders and pathogeneses.[8–10,23,29]

We identified that hyperactivation of ERVs leads to severe cardiac inflammation, cell death, and AHF in TRIM28^{iCKO} mice, which resembles myocarditis in the clinical setting. Myocarditis, especially fulminant myocarditis, is one of the leading causes of AHF, with mortality rates as high as 80%, affecting juveniles and young people.[40] Myocarditis is typically caused by infection with exogeneous viruses, such as adenoviruses and retroviruses.[3,4] For example, COVID-19, as a retrovirus, was associated with a significant increase in myocarditis and cardiomyopathy during the pandemic.[41] Different from exogenous viral infection, we find that the aberrant expression of endogenous ERV nucleic acids also induces acute and severe myocarditis. Intriguingly, several studies also showed that exogenous virus infection is one of the prominent stimuli for ERV reactivation.[42] Collectively, these findings suggest that ERVs may play a broader role in exogenous viral infection–induced myocarditis. Of note, a recent porcine-to-human heart xenotransplantation trial indicated that the failure of xenografts may be associated with the resurgence of porcine ERV and cytomegalovirus.[43] In the present study, we identify that ERVs and their activation of innate immunity play an important role in I/R-induced myocarditis and HF. These results together underscore ERVs as pivotal pathogens with pervasive roles in myocarditis and HF.

ERVs have to be rigorously silenced to prevent genomic instability and aberrant transcription.[6–8] Over millions of years, vertebrates have evolved variable mechanisms to maintain ERV surveillance in the genome, such as DNA erosion and methylation, histone modifications, and transcription factor repression. Recent studies found that these mechanisms can be highly specific to tissue type, developmental stage, and genomic context.[26] Here, we found that ERV silence in the myocardium is orchestrated by TRIM28, based on the key observation that cardiomyocyte-specific genetic deletion of TRIM28 leads to an obvious ERV resurgence that further results in acute myocarditis and severe HF. Conversely, restoring TRIM28 in the failing heart resilences ERVs and improves heart function. The effectiveness of TRIM28 in shutting down ERVs may be attributable to its dual function to simultaneously regulate both H3K9me3 and RNA m^{6}A, which is different from its canonical and singular role in maintaining H3K9me3 on ERV genomes discovered in other tissues.[32] This mechanistic difference reinforces the notion about the regulatory specificity of ERVs, highlighting their unique role in cardiac homeostasis and dysfunction.

TLR7/9 are two key TLR receptors that recognize exogenous nucleic acid pathogen-associated molecular pattern ligands (RNA and DNA) to incur innate immunity. The sustained or constant activation of TLR7/9 can lead to hyperactivation of inflammation, contributing to autoimmune disorders such as systemic lupus erythematosus. Here, we illustrate another important role of

TLR7/9 in myocarditis and ischemic HF, to sense the activated ERVs, suggesting their broad immunological significance. cGAS, another cytosolic sensor for exogenous double-stranded DNA, is also upregulated in TRIM28-depleted hearts. However, cGAS is less effective than TLR7/9 in rescuing cardiac function. This observation further supports the theory that the ERV-sensing mechanism in cardiomyocytes is biased toward TLR7/9. Several reasons may be attributed to this bias, including a lower abundance of double-stranded DNA than single-stranded RNA or single-stranded DNA derived from ERVs, higher expression of TLR7/9, or biased composition and interactome of myddosome in cardiomyocytes. Something similar is observed as well in the expression dissociation of cytokines and IFN. These data emphasize the unique feature of innate immune signal transduction pathways in cardiomyocytes. Moreover, NSC4375, as a small-molecule inhibitor of TLR7/9, has been employed in therapeutic regimens for SLE, and rheumatoid arthritis, autoimmune myocarditis and reduces COVID-19 mortality by inhibiting innate immunity.[44,45] The notable efficacy of NSC4375 in cardiac protection against I/R injury, as illustrated by our study, also suggest its broader therapeutic potential in treating myocarditis and cardiomyopathy. However, to rule out the effects of sex hormones on cardiac protection, only male mice were used in the I/R model, representing a potential limitation. Whether these findings can be recapitulated in female mice requires further examination.

In summary, our study defines the previously unrecognized pathological pathway of TRIM28–ERV–TLR7/9–NF-κB in myocarditis and HF, which provides new mechanistic insights and therapeutic perspectives for these illnesses. We also identify ERV resurgence as a key driver of cardiac inflammation and dysfunction, which highlights the critical role of viral-host genome interaction in HF pathogenesis.

ARTICLE INFORMATION

Received March 30, 2025; accepted July 22, 2025.

Affiliations

Key Laboratory of Systems Biomedicine, Shanghai Center for Systems Biomedicine, Department of Cardiovascular Surgery, Shanghai Chest Hospital, Engineering Research Center of Techniques and Instruments for Diagnosis and Treatment of Congenital Heart Disease, Institute of Developmental and Regenerative Medicine, Xin Hua Hospital, School of Medicine, Shanghai Jiao Tong University, Shanghai, China (J.X., S.Z., Z.G., J.L., K.C., H.H., Y.W., Y.S., P.Y., Yige Li, S.W., X.C., A.F.C., X.H., R.L., D.Z., K.S., B.Z.). Basic Medical Research Center, Second Affiliated Hospital and Yuying Children's Hospital of Wenzhou Medical University, Wenzhou, Zhejiang, China (X.L., X.G.). Department of Pharmacology, School of Medicine, Southern University of Science and Technology, Shenzhen, China (Yelan Li, Y.F.). State Key Laboratory of Genetic Engineering, Human Phenome Institute, Department of Anthropology and Human Genetics, School of Life Sciences and Zhongshan Hospital, Fudan University, Shanghai, China (A.S.). Division of Cardiology, Department of Internal Medicine, Tongji Hospital, Tongji Medical College (D.W., C.C.). School of Biomedical Engineering, Shanghai Jiao Tong University, Shanghai, China (Y.Z.). Department of Cardiology, Chongqing Institute of Cardiology, Chongqing Cardiovascular Clinical Research Center, Daping Hospital (G.W., C.Z.).

Acknowledgments

The authors thank Dr Xiaoyu Tian (Heart and Vascular Institute, The Chinese University of Hong Kong) for elaborative revision, Dr Jiekai Chen (Guangzhou Institutes of Biomedicine and Health, Chinese Academy of Sciences) for kindly providing SETDB1 animals, and Dr Chengqi Yi (State Key Laboratory of Protein and Plant Gene Research, School of Life Sciences, Peking University, Beijing, China) for m^{6}A analysis, and the Laboratory Animal Center and Instrumental Analysis Center of Shanghai Jiao Tong University for technical support.

Sources of Funding

This work was supported by the National Key Research and Development Program of China (2020YFA0803800, 2020YFA0803802, 2023YFA1800700, 2023YFA1800702, and 2023YFA1800703), the National Foundation of Distinguished Young Scholars of China (82225006), the National Natural Science Foundation of China (NSFC 32200926), the Innovation Program of the Shanghai Municipal Education Commission (2021-01-07-00-02-E00088), SJTU Transmed Awards Research (STAR) awards (YG2022ZD023, YG2023QNB13, and YG2025QNB40), the Young Scientific Research Special Fund (KLSB2022QN-03), and the Natural Science Foundation of Shanghai under the 2024 Shanghai Action Plan for Science, Technology, and Innovation (24ZR1439200).

Disclosures

None.

Supplemental Materials

ARRIVE Checklist
Supplemental Methods
Figures S1–S10
Tables S1–S7
References 46–50

REFERENCES

1. Savarese G, Becher PM, Lund LH, Seferovic P, Rosano GMC, Coats AJS. Global burden of heart failure: a comprehensive and updated review of epidemiology. *Cardiovasc Res*. 2023;118:3272–3287. doi: 10.1093/cvr/cvac013
2. Hernandez AF, Granger CB. Advancing care for acute heart failure--no time to relax. *Lancet*. 2009;373:1401–1402. doi: 10.1016/S0140-6736(09)60653-X
3. Tschope C, Ammirati E, Bozkurt B, Caforio ALP, Cooper LT, Felix SB, Hare JM, Heidecker B, Heymans S, Hubner N, et al. Myocarditis and inflammatory cardiomyopathy: current evidence and future directions. *Nat Rev Cardiol*. 2021;18:169–193. doi: 10.1038/s41569-020-00435-x
4. Hang W, Chen C, Seubert JM, Wang DW. Fulminant myocarditis: a comprehensive review from etiology to treatments and outcomes. *Signal Transduct Target Ther*. 2020;5:287. doi: 10.1038/s41392-020-00360-y
5. Lanciano S, Cristofari G. Measuring and interpreting transposable element expression. *Nat Rev Genet*. 2020;21:721–736. doi: 10.1038/s41576-020-0251-y
6. Stocking C, Kozak CA. Murine endogenous retroviruses. *Cell Mol Life Sci*. 2008;65:3383–3398. doi: 10.1007/s00018-008-8497-0
7. Geis FK, Goff SP. Silencing and transcriptional regulation of endogenous retroviruses: an overview. *Viruses*. 2020;12:884. doi: 10.3390/v12080884
8. Dopkins N, Nixon DF. Activation of human endogenous retroviruses and its physiological consequences. *Nat Rev Mol Cell Biol*. 2024;25:212–222. doi: 10.1038/s41580-023-00674-z
9. Jakobsson J, Vincendeau M. SnapShot: human endogenous retroviruses. *Cell*. 2022;185:400–400.e1. doi: 10.1016/j.cell.2021.12.028
10. Kassiotis G, Stoye JP. Immune responses to endogenous retroelements: taking the bad with the good. *Nat Rev Immunol*. 2016;16:207–219. doi: 10.1038/nri.2016.27
11. Iyengar S, Farnham PJ. KAP1 protein: an enigmatic master regulator of the genome. *J Biol Chem*. 2011;286:26267–26276. doi: 10.1074/jbc.R111.252569
12. Cheng CT, Kuo CY, Ann DK. KAPtain in charge of multiple missions: emerging roles of KAP1. *World J Biol Chem*. 2014;5:308–320. doi: 10.4331/wjbc.v5.i3.308
13. Seki Y, Kurisaki A, Watanabe-Susaki K, Nakajima Y, Nakanishi M, Arai Y, Shiota K, Sugino H, Asashima M. TIF1beta regulates the pluripotency of embryonic stem cells in a phosphorylation-dependent manner. *Proc Natl Acad Sci U S A*. 2010;107:10926–10931. doi: 10.1073/pnas.0907601107
14. Jakobsson J, Cordero MI, Bisaz R, Groner AC, Busskamp V, Bensadoun JC, Cammas F, Losson R, Mansuy IM, Sandi C, et al. KAP1-mediated epigenetic

repression in the forebrain modulates behavioral vulnerability to stress. *Neuron*. 2008;60:818–831. doi: 10.1016/j.neuron.2008.09.036
15. Ma X, Yang T, Luo Y, Wu L, Jiang Y, Song Z, Pan T, Liu B, Liu G, Liu J, et al. TRIM28 promotes HIV-1 latency by SUMOylating CDK9 and inhibiting P-TEFb. *Elife*. 2019;8:e42426. doi: 10.7554/eLife.42426
16. Brattas PL, Jonsson ME, Fasching L, Nelander Wahlestedt J, Shahsavani M, Falk R, Falk A, Jern P, Parmar M, Jakobsson J. TRIM28 Controls a gene regulatory network based on endogenous retroviruses in human neural progenitor cells. *Cell Rep*. 2017;18:1–11. doi: 10.1016/j.celrep.2016.12.010
17. Chikuma S, Yamanaka S, Nakagawa S, Ueda MT, Hayabuchi H, Tokifuji Y, Kanayama M, Okamura T, Arase H, Yoshimura A. TRIM28 expression on dendritic cells prevents excessive T cell priming by silencing endogenous retrovirus. *J Immunol*. 2021;206:1528–1539. doi: 10.4049/jimmunol.2001003
18. Matsui T, Leung D, Miyashita H, Maksakova IA, Miyachi H, Kimura H, Tachibana M, Lorincz MC, Shinkai Y. Proviral silencing in embryonic stem cells requires the histone methyltransferase ESET. *Nature*. 2010;464:927–931. doi: 10.1038/nature08858
19. Liang X, Wu S, Geng Z, Liu L, Zhang S, Wang S, Zhang Y, Huang Y, Zhang B. LARP7 suppresses endothelial-to-mesenchymal transition by coupling with TRIM28. *Circ Res*. 2021;129:843–856. doi: 10.1161/CIRCRESAHA.121.319590
20. Li H, Fan J, Zhao Y, Zhang X, Dai B, Zhan J, Yin Z, Nie X, Fu XD, Chen C, et al. Nuclear miR-320 mediates diabetes-induced cardiac dysfunction by activating transcription of fatty acid metabolic genes to cause lipotoxicity in the heart. *Circ Res*. 2019;125:1106–1120. doi: 10.1161/CIRCRESAHA.119.314898
21. Wu K, Liu H, Wang Y, He J, Xu S, Chen Y, Kuang J, Liu J, Guo L, Li D, et al. SETDB1-mediated cell fate transition between 2C-like and pluripotent states. *Cell Rep*. 2020;30:25–36.e6. doi: 10.1016/j.celrep.2019.12.010
22. Heckmann MB, Finke D, Sauerbrey L, Frey N, Lehmann LH. Increased expression of human endogenous retrovirus K in endomyocardial biopsies from patients with cardiomyopathy: a transcriptomics meta-analysis. *BMC Genomics*. 2024;25:707. doi: 10.1186/s12864-024-10595-6
23. Licastro F, Porcellini E. Activation of endogenous retrovirus, brain infections and environmental insults in neurodegeneration and Alzheimer's disease. *Int J Mol Sci* . 2021;22:7263. doi: 10.3390/ijms22147263
24. Grandi N, Tramontano E. Type W human endogenous retrovirus (HERV-W) integrations and their mobilization by L1 machinery: contribution to the human transcriptome and impact on the host physiopathology. *Viruses*. 2017;9:162. doi: 10.3390/v9070162
25. Dendrou CA, Fugger L, Friese MA. Immunopathology of multiple sclerosis. *Nat Rev Immunol*. 2015;15:545–558. doi: 10.1038/nri3871
26. Jonsson ME, Garza R, Johansson PA, Jakobsson J. Transposable elements: a common feature of neurodevelopmental and neurodegenerative disorders. *Trends Genet*. 2020;36:610–623. doi: 10.1016/j.tig.2020.05.004
27. Xu W, Li J, He C, Wen J, Ma H, Rong B, Diao J, Wang L, Wang J, Wu F, et al. METTL3 regulates heterochromatin in mouse embryonic stem cells. *Nature*. 2021;591:317–321. doi: 10.1038/s41586-021-03210-1
28. Zhang SM, Cai WL, Liu X, Thakral D, Luo J, Chan LH, McGeary MK, Song E, Blenman KRM, Micevic G, et al. KDM5B promotes immune evasion by recruiting SETDB1 to silence retroelements. *Nature*. 2021;598:682–687. doi: 10.1038/s41586-021-03994-2
29. Garen A. From a retrovirus infection of mice to a long noncoding RNA that induces proto-oncogene transcription and oncogenesis via an epigenetic transcription switch. *Signal Transduct Target Ther*. 2016;1:16007. doi: 10.1038/sigtrans.2016.7
30. Costain WJ, Rasquinha I, Graber T, Luebbert C, Preston E, Slinn J, Xie X, MacManus JP. Cerebral ischemia induces neuronal expression of novel VL30 mouse retrotransposons bound to polyribosomes. *Brain Res*. 2006;1094:24–37. doi: 10.1016/j.brainres.2006.03.120
31. Wang X, Lu Z, Gomez A, Hon GC, Yue Y, Han D, Fu Y, Parisien M, Dai Q, Jia G, et al. N6-methyladenosine-dependent regulation of messenger RNA stability. *Nature*. 2014;505:117–120. doi: 10.1038/nature12730
32. Rowe HM, Jakobsson J, Mesnard D, Rougemont J, Reynard S, Aktas T, Maillard PV, Layard-Liesching H, Verp S, Marquis J, et al. KAP1 controls endogenous retroviruses in embryonic stem cells. *Nature*. 2010;463:237–240. doi: 10.1038/nature08674
33. Patil DP, Pickering BF, Jaffrey SR. Reading m(6)A in the transcriptome: m(6)A-binding proteins. *Trends Cell Biol*. 2018;28:113–127. doi: 10.1016/j.tcb.2017.10.001
34. Dominissini D, Moshitch-Moshkovitz S, Schwartz S, Salmon-Divon M, Ungar L, Osenberg S, Cesarkas K, Jacob-Hirsch J, Amariglio N, Kupiec M, et al. Topology of the human and mouse m6A RNA methylomes revealed by m6A-seq. *Nature*. 2012;485:201–206. doi: 10.1038/nature11112
35. Liu J, Yue Y, Han D, Wang X, Fu Y, Zhang L, Jia G, Yu M, Lu Z, Deng X, et al. A METTL3-METTL14 complex mediates mammalian nuclear RNA N6-adenosine methylation. *Nat Chem Biol*. 2014;10:93–95. doi: 10.1038/nchembio.1432
36. O'Neill LA, Bryant CE, Doyle SL. Therapeutic targeting of Toll-like receptors for infectious and inflammatory diseases and cancer. *Pharmacol Rev*. 2009;61:177–197. doi: 10.1124/pr.109.001073
37. De Cecco M, Ito T, Petrashen AP, Elias AE, Skvir NJ, Criscione SW, Caligiana A, Brocculi G, Adney EM, Boeke JD, et al. L1 drives IFN in senescent cells and promotes age-associated inflammation. *Nature*. 2019;566:73–78. doi: 10.1038/s41586-018-0784-9
38. Goodier JL, Kazazian HH Jr. Retrotransposons revisited: the restraint and rehabilitation of parasites. *Cell*. 2008;135:23–35. doi: 10.1016/j.cell.2008.09.022
39. Mandal PK, Kazazian HH Jr. SnapShot: vertebrate transposons. *Cell*. 2008;135:192–192.e1. doi: 10.1016/j.cell.2008.09.028
40. Wu J, Lu AD, Zhang LP, Zuo YX, Jia YP. Study of clinical outcome and prognosis in pediatric core binding factor-acute myeloid leukemia. *Zhonghua Xue Ye Xue Za Zhi*. 2019;40:52–57. doi: 10.3760/cma.j.issn.0253-2727.2019.01.010
41. Ono R, Iwahana T, Aoki K, Kato H, Okada S, Kobayashi Y. Fulminant myocarditis with SARS-CoV-2 Infection: a narrative review from the case studies. *Can J Infect Dis Med Microbiol*. 2024;2024:9000598. doi: 10.1155/2024/9000598
42. Zhang L, Richards A, Barrasa MI, Hughes SH, Young RA, Jaenisch R. Reverse-transcribed SARS-CoV-2 RNA can integrate into the genome of cultured human cells and can be expressed in patient-derived tissues. *Proc Natl Acad Sci U S A*. 2021;118: doi: 10.1073/pnas.2105968118
43. Griffith BP, Goerlich CE, Singh AK, Rothblatt M, Lau CL, Shah A, Lorber M, Grazioli A, Saharia KK, Hong SN, et al. Genetically modified porcine-to-human cardiac xenotransplantation. *N Engl J Med*. 2022;387:35–44. doi: 10.1056/NEJMoa2201422
44. Lee SJ, Silverman E, Bargman JM. The role of antimalarial agents in the treatment of SLE and lupus nephritis. *Nat Rev Nephrol*. 2011;7:718–729. doi: 10.1038/nrneph.2011.150
45. Yu B, Li C, Chen P, Zhou N, Wang L, Li J, Jiang H, Wang DW. Low dose of hydroxychloroquine reduces fatality of critically ill patients with COVID-19. *Sci China Life Sci*. 2020;63:1515–1521. doi: 10.1007/s11427-020-1732-2
46. Yu H, Zhang F, Yan P, Zhang S, Lou Y, Geng Z, Li Z, Zhang Y, Xu Y, Lu Y, et al. LARP7 protects against heart failure by enhancing mitochondrial biogenesis. *Circulation*. 2021;143:2007–2022. doi: 10.1161/CIRCULATIONAHA.120.050812
47. Ackers-Johnson M, Li PY, Holmes AP, O'Brien SM, Pavlovic D, Foo RS. A simplified, Langendorff-free method for concomitant isolation of viable cardiac myocytes and nonmyocytes from the adult mouse heart. *Circ Res*. 2016;119:909–920. doi: 10.1161/CIRCRESAHA.116.309202
48. Yan P, Li Z, Xiong J, Geng Z, Wei W, Zhang Y, Wu G, Zhuang T, Tian X, Liu Z, et al. LARP7 ameliorates cellular senescence and aging by allosterically enhancing SIRT1 deacetylase activity. *Cell Rep*. 2021;37:110038. doi: 10.1016/j.celrep.2021.110038
49. Love MI, Huber W, Anders S. Moderated estimation of fold change and dispersion for RNA-seq data with DESeq2. *Genome Biol*. 2014;15:550. doi: 10.1186/s13059-014-0550-8
50. Jin Y, Tam OH, Paniagua E, Hammell M. TEtranscripts: a package for including transposable elements in differential expression analysis of RNA-seq datasets. *Bioinformatics*. 2015;31:3593–3599. doi: 10.1093/bioinformatics/btv422